An Integrative Overview of the Open Literature's Empirical Data on In-tunnel Radiowave Propagation's Power Loss

by

Le Li

A thesis

presented to the University of Waterloo

in fulfillment of the

thesis requirement of the degree of

Master of Applied Science

in

Electrical and Computer Engineering

Waterloo, Ontario, Canada, 2006

I hereby declare that I am the sole author of this thesis. This is a true copy of the thesis, including any required final revisions, as accepted by my examiners.

I understand that my thesis may be made electronically available to the public.

Le Li

Abstract

This paper offers a comprehensive and integrative overview of all empirical data available from the open literature on the in-tunnel radiowave-communication channel's power loss characteristics, as a function of the tunnel's cross-sectional shape, cross-sectional size, longitudinal shape, wall materials, presence or absence of vehicular/human traffic, and presence/absence of branches. These data were originally presented in about 50 papers in various journals, conferences, and books.

Acknowledgments

I thank my supervisor, Prof. K. T. Wong for giving me inspiration and guidance during my course work as well as research. I grew to respect Prof. Wong for his intellect and his unlimited enthusiasm and support to his students.

I also thank my family for their constant support, backing, and encouragement throughout my studies and research.

Contents

List of Tables

List of Figures

Chapter 1

Introduction

Characterization of radiowave wireless propagation in indoor environments has focused largely on homes, offices, or factories. Relatively neglected are tunnels -- mining tunnels, highway road tunnels, urban subway tunnels, etc. Automobile road highways, railways, and urban subways often include tunnel sections, or cuttings to mitigate noise pollution to neighborhoods around the highway. Mountainous Austria has 10% of its priority roads in tunnels [13]; and Taiwan's North Second Freeway has 23 tunnels with a total length of 15.88 kilometers [18].

Leaky feeder cables have been customarily been used inside tunnels. Voice communication is provided by stringing wires over the length of the tunnel, or by placing repeaters at intervals, or both. These methods are expensive to install (especially after the tunnel has been opened for public use), are inconvenient, need regular maintenance, could be unreliable in disasters or fires or terrorist situations, and do not allow an in-tunnel mobile user to transmit (as opposed to receiving). Wireless communications, using ``discrete'' antennas for transceivers inside tunnels, can avoid all above shortcomings, with the added a possible advantage of needing no prior infra-structure in peer-to-peer wireless communications.

The use for in-tunnel wireless communications is varied: cell-phones for pedestrians in underground streets, cell phones for riders in subways, command-and-control signaling between a mobile rail-car and stationary base-station inside deep mine shafts, remote electronic surveillance on-board the rail-car from a base-station, or

high-reliability communications in emergencies such as fires or terrorism. In these scenarios, the transceiver could be a stationary base-station, a mobile station on a train, or a paying user's cell-phone.

Long-range in-tunnel radio communication's viability, coverage, and quality depend critically on the in-tunnel radio propagation's power loss. Ordinary indoor cell-planning is inapplicable to tunnels, due to the serious wave-guiding effects inside tunnels.

Tunnels could be electromagnetically idealized as over-sized imperfect dielectric waveguides with many indeterminable higher-order propagation modes, but the irregularities in a real-world tunnel render mathematical electromagnetic prediction difficult and inaccurate. Simple electromagnetic dielectric waveguide theory might be insufficient, due to the tunnel's complicated shape (e.g., tilting and curved side walls, uneven cross-section along the tunnel's longitude, variable longitudinal curvature, auxiliary branched tunnels, cross-tunnels, and inter-connected galleries, temporally changing layout as ores are mined and removed), the tunnel's variable wall surfaces (e.g., variable wall roughness[1] , the side-walls and ceiling and floor being made of different materials), and the in-tunnel obstacles (e.g., irregular pillars, trolley wires and rails, shuttle cars, mining machinery, rock debris in a mine, highly variable in-tunnel vehicular and human traffic conditions, other irregularly in-tunnel scatterers of arbitrary electromagnetic properties). In-tunnel radiowave propagation could be measured empirically and then characterized statistically.

The study aims for such a statistical characterization of the in-tunnel power loss, to present simple rules-of-thumb without explicit reference to the Maxwell equations.

---

[1] While the mine tunnel's side walls may be rough relative to the wavelength, the mine tunnel's ceiling and floor are reasonably flat and level.

The tunnel is a transmission channel of high-pass type. If the radio signal frequency is lower than the tunnel cutoff frequency, propagation will suffer considerable attenuation. On the other hand, if the radio-signal frequency is much higher than the tunnel cutoff frequency, propagation will attenuate less than that in free-space [24]. It is found that the higher the frequency, the smaller the attenuation constant [2].

A theoretical model based on the modal theory has been proposed to explain tunnel guiding propagation characteristics [13]-[15]. This model treats a tunnel as a hollow oversized imperfect waveguide. Propagation is governed by a fundamental mode and an infinite number of higher order modes. The model is complicated because the coupling of these modes arises due to the imperfection of the waveguide. Another theoretical model based on the geometrical optic theory was then proposed [16]. The geometrical optic theory considers the tunnel walls as reflected planes. Propagation is achieved via a direct path and all possible reflected paths. Both theories are restricted to empty straight tunnels and, thus, have limitations [24].

Modal theory, assuming a straight tunnel with perfectly smooth walls, would have attenuation to drop with decreasing wavelength. Attenuation is lower if the tunnel's transverse dimensions greatly exceed the wavelength, with the tunnel behaving as a lossy oversized wavelength supporting hybrid modes.

An electromagnetic wave traveling along a rectangular tunnel in a dielectric medium can propagate in any one of a number of allowed waveguide modes. All of these modes are "lossy modes" owing to the fact that any part of the wave that impinges on a wall of the tunnel is partially refracted into the surrounding dielectric and partially reflected back into the waveguide. The refracted part propagates away from the waveguide and represents a power loss [1]. Rather than being reflected, lower-frequency signals tend to be absorbed by the tunnel walls more than higher-frequency signals. Metal tunnels would reflect more energy than it absorbs,

and a concrete tunnel would be vice versa thereby decreasing the distance the signal can propagate down the tunnel.

In the vicinity of the transmitter there are important fluctuations due to the contribution of all high-order modes excited by the transmitting antenna while, at a large distance, the low-order modes become dominant and the attenuation per unit length becomes much smaller [30].

At higher frequencies and in much wider tunnels, the field distribution far from the transmitter would present fast fluctuations, the high-order modes being not too much attenuated [30].

A tunnel's longitudinal curves can decrease signal power due to blockage of the LOS paths.

Radio signal propagation in a tunnel exhibits distinct near and far regions with quite different propagation characteristics. In the short distance region, more significant reflected rays cause large fluctuations, whereas in the long distance region as the reflected rays become less significant, the direct ray contributes the most to the received signal. Therefore, the magnitude of fluctuations diminishes as the receiver moves further away from the transmitter. Both measurements and predictions show the existence of a distinct break point along the line-of-sight path, before and after which the propagation has different rate of attenuation. This propagation behavior was observed in other radio environments as well. The method of determining the location of the break point was given in [19], which can estimate the position of the break point in tunnel environments [24].

We define the intersection as the break point to distinguish the propagation regions. Before the break point is the near propagation region, which has the first Fresnel zone

clearance. The propagation takes place in this region of the tunnel as if it were in free space; the propagation loss is, therefore, calculated by the single ray optical (free space) model. After the break point is the far propagation region, where the constructive interference dominates; the propagation takes place in this region of the tunnel as if it were in a waveguide. The propagation loss is, therefore, calculated by the analytical ray optical (waveguide) model [41]. The near-zone extends further in axial distance as the frequency increases [47]. It has many modes interacting for rapid decay and strong local variations. In the far zone, only a few principal modes (or just one mode) dominate with less rapid decay and smother local variations. As the tunnel cross-section decreases in size, the break point will occur at a smaller distance from the transmitter, as the high-order modes would be more attenuated.

Chapter 2

Overview of Empirical Data

Notations:

Symbol	Definition
P_L	Power loss (dB)
D	Transmitter-receiver distance (meter)
λ	Wavelength
W	Width of tunnel cross-section / λ
H	Height of tunnel cross-section / λ
C_{Tx}	$\min\{\frac{x}{W}, \frac{y}{H}, \frac{W-x}{W}, \frac{H-y}{H}\}$, where (x, y) is the transmitter's coordinates on the cross-section
C_{Rx}	$\min\{\frac{x}{W}, \frac{y}{H}, \frac{W-x}{W}, \frac{H-y}{H}\}$, where (x, y) is the receiver's coordinates on the cross-section
A	$\frac{WH}{\lambda^2}$, Normalized area of tunnel cross-section
R	$\frac{W}{H}$
VV	Both transmitter and receiver are vertically polarized
HH	Both transmitter and receiver are horizontally polarized
BP	Break point (meter)
BBP	Before break point
ABP	After break point
α	The ratio of $\frac{P_L}{D/\lambda}(BBP)$ to $\frac{P_L}{D/\lambda}(ABP)$
T_w	$\frac{x}{W}$, where x is the transmitter's coordinate for x-axis
T_h	$\frac{y}{H}$, where y is the transmitter's coordinate for y-axis
R_w	$\frac{x}{W}$, where x is the receiver's coordinate for x-axis
R_h	$\frac{y}{H}$, where y is the transmitter's coordinate for y-axis

2.1 Straight-Rectangular-Empty Tunnels

Figure 2-1-A: BBP part of Road or Concrete tunnels

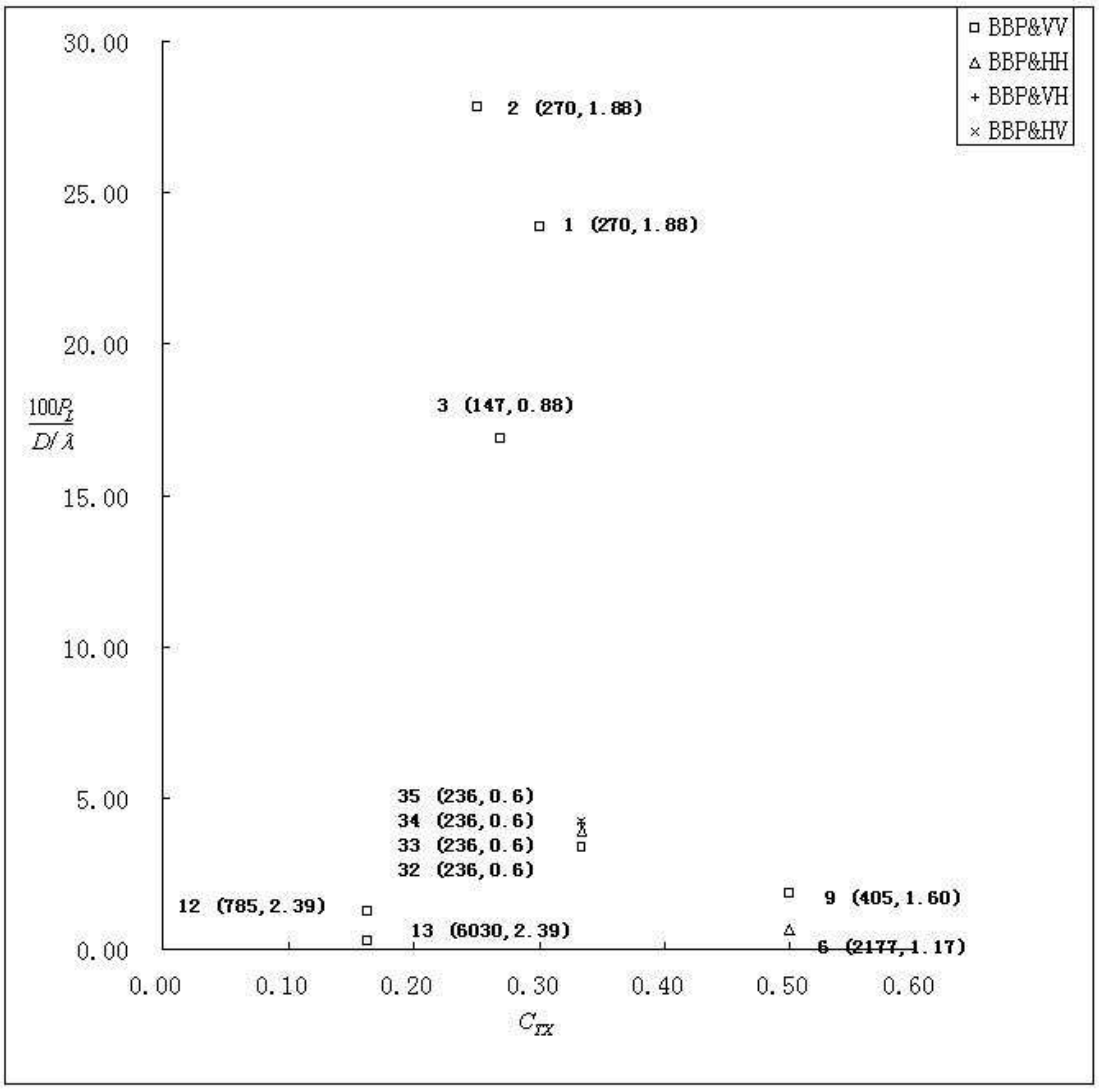

Observations:

- The data sets' structure is (A, R).
- $\frac{P_L}{D/\lambda}$ decreases with increasing A. This can be concluded from data sets {#12, #13}. This agrees with the empirical trend by [20], which says $\frac{P_L}{D/\lambda}$ decreases with decreasing wavelength.
- Noting that the only difference between data sets {#1, #2} is C_{Tx}. $\frac{P_L}{D/\lambda}$ for $C_{Tx} = 0.3$ less than that for $C_{Tx} = 0.25$. It is claimed in [20] that as $C_{Tx} \to 0.5$, the "insertion loss" is minimized. So the conclusion: $\frac{P_L}{D/\lambda}(C_{Tx} = 0.5) < \frac{P_L}{D/\lambda}(C_{Tx} \neq 0.5)$

- $\frac{P_L}{D/\lambda}$ decreases when the cross-sectional shape matches the linear polarization of electric field as follows: For VV, $\frac{P_L}{D/\lambda}$ decreases with decreasing R. For HH, $\frac{P_L}{D/\lambda}$ decreases with increasing R. This can be concluded from data sets {#1, #3}, where data set #1's larger A and $C_{Tx} = 0.3$ would have produced a smaller $\frac{P_L}{D/\lambda}$, but for data set #1's large R. The present authors think that this is because as R increases, the shorter will be in the vertical direction of cross-section. This will produce a larger $\frac{P_L}{D/\lambda}$ for vertical polarization than horizontal polarization, due to more reflections and refractions for vertical polarization.
- The relation between $\frac{P_L}{D/\lambda}$ and R can be further demonstrated from data sets {#32, #33}. For both data sets, R < 1, which means the height exceeds the width for these two cross-sections. As discussed above, such a cross-section better suits vertical polarization, thus data set #32, whose polarization is vertical, has a lower $\frac{P_L}{D/\lambda}$ than data set #33, whose polarization is horizontal. Data sets {#1, #32} also agree with this conclusion.
- Mismatching the linear polarization of electric field between transmitter and receiver can produce extra loss in $\frac{P_L}{D/\lambda}$. This can be seen from data sets {#32, #33, #34, #35}. All these data are from the same tunnel, and data sets {#34, #35}, whose polarization is mismatched, have a bigger $\frac{P_L}{D/\lambda}$ than that for the data sets {#32, #33}, whose polarization is matched.
- The effect of mismatching in the linear polarization of electric field between transmitter and receiver increases with increasing A. In tunnel environment, signal fading is mainly due to reflections and refractions. As A increasing, fading related to reflections and refractions decreases. Hence, polarization mismatching between transmitter and receiver becomes more important. This can be seen from data sets {#33, #34}. The transmitter in #33 sending horizontal signal, would have a bigger $\frac{P_L}{D/\lambda}$ than #34, which sends vertical signal, in a tunnel whose R is less than 1, but for the polarization mismatch between transmitter and receiver in #34 and the relatively big A. Later, an example will be presented to show that in a tunnel whose A is small, polarization mismatch between transmitter and receiver does not affect too much.
- The effect of mismatch between polarization and cross-sectional shape decreases with increasing A. The reason is still as A increasing, signal fading due to reflections and refractions decreases, so the mismatch between cross-sectional

shape and polarization does not affect too much. This can be seen from data sets {#6, #13}. #6's horizontal polarization would have a smaller $\frac{P_L}{D/\lambda}$ than that for #13 in tunnels whose R is bigger than 1, but for the #13' larger A.

Figure 2-1-B: ABP part of Road or Concrete tunnels

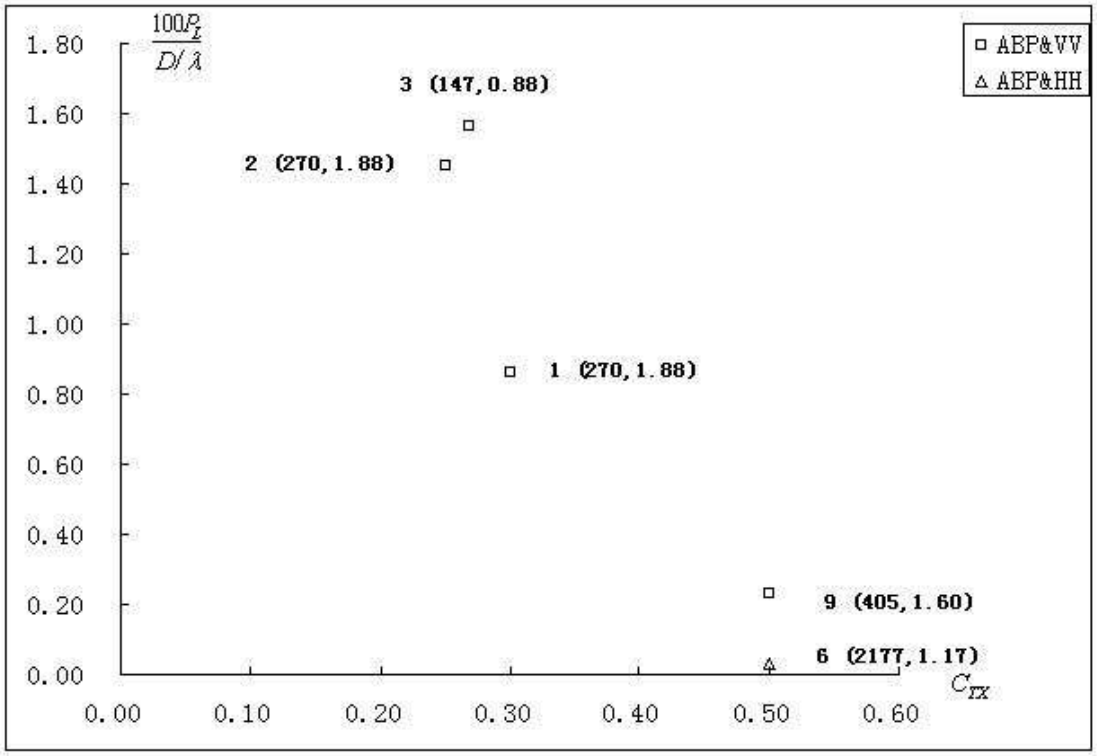

Observations:

- $\frac{P_L}{D/\lambda}$'s typical values and variations are smaller for ABP than for BBP. This can be concluded from comparing the values between Fig. 2-1-A and Fig. 2-1-B and can be explained as follows: ABP part of a straight tunnel is the far distance region to the transmitter compared with BBP part. In ABP part, LOS signal dominates the transmission; the effect of multi-path components is weakened compared with BBP part, due to many reflections and refractions, so less fluctuation leads a smaller $\frac{P_L}{D/\lambda}$ in ABP part of a tunnel than BBP part. This agrees with the conclusion in [20].
- $\frac{P_L}{D/\lambda}$ for $C_{Tx}=0.3$ is less than that for $C_{Tx}=0.25$. It can be concluded from data sets {#1, #2}. This also agrees with previous conclusion in Fig. 2-1-A:

  $$\frac{P_L}{D/\lambda}(C_{Tx}=0.5) < \frac{P_L}{D/\lambda}(C_{Tx}\neq 0.5)$$
- The effect of R is weakened in ABP part of tunnel than BBP part. This can be seen from data sets {#1, #2, #3}. Unlike in Fig. 2-1-A, #1 and #2's bigger A gives them a smaller $\frac{P_L}{D/\lambda}$ than #3, despite #3's smaller R.
- Data sets {#1, #2, #9} agree with the conclusion:

  $$\frac{P_L}{D/\lambda}(C_{Tx}=0.5) < \frac{P_L}{D/\lambda}(C_{Tx}\neq 0.5)$$

Figure 2-1-C: BBP part of Coal Mine tunnels

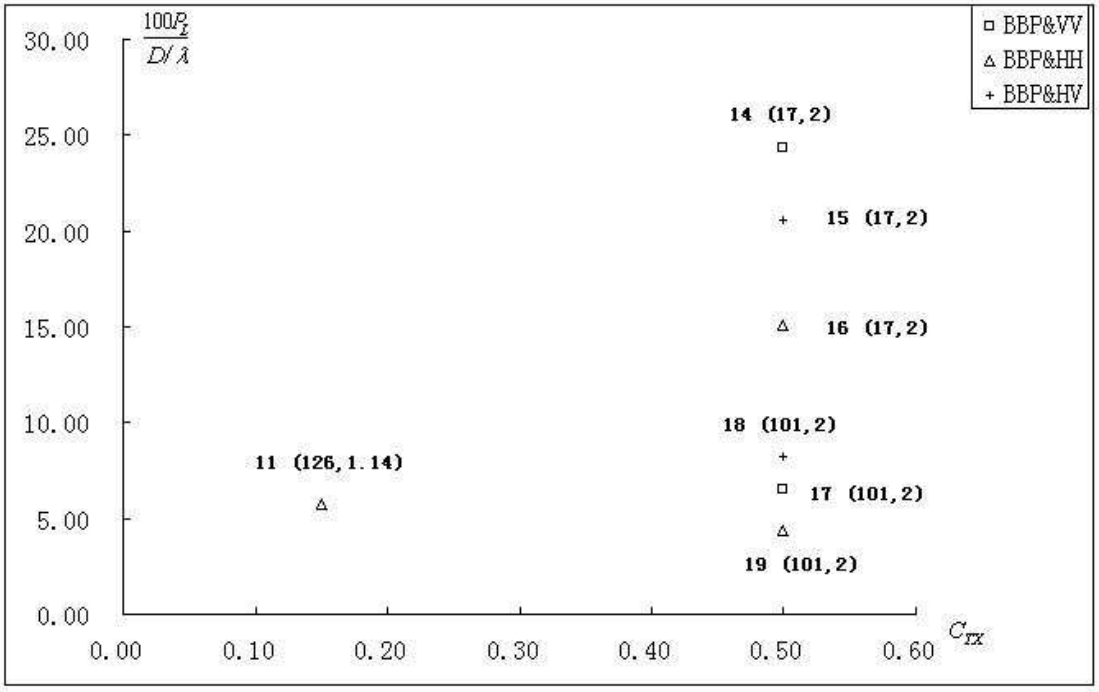

Observations:

- $\frac{P_L}{D/\lambda}$ decreases with increasing A, by comparing data sets #14 against #17, or #15 against #18, or #16 against #19
- $\frac{P_L}{D/\lambda}$ decreases when the cross-sectional shape matches the linear polarization of electric field: data sets {#14, #16}, or {#17, #19}.
- Mismatching the linear polarization of electric field between transmitter and receiver can lead extra loss in $\frac{P_L}{D/\lambda}$: data sets {#15, #16}, or {#18, #19}.
- The effect of mismatching in the linear polarization of electric field between transmitter and receiver increases with increasing A. This can be seen from data sets {#14, #15}, and {#17, #18}. The polarization mismatching in #15 (HV) is not important compared with #14, which is vertically polarized, in a small tunnel, with R bigger than 1. The reason is that the signal attenuation in this small tunnel is mainly due to reflections and refractions so that the effect of mismatching in the linear polarization of electric field between transmitter and receiver is weakened. On the other hand, data sets {#17, #18} are in a big tunnel, so the attenuation due to reflections is decreased, hence, the polarization mismatching becomes important in this case.

Figure 2-1-D: ABP part of Coal Mine tunnels

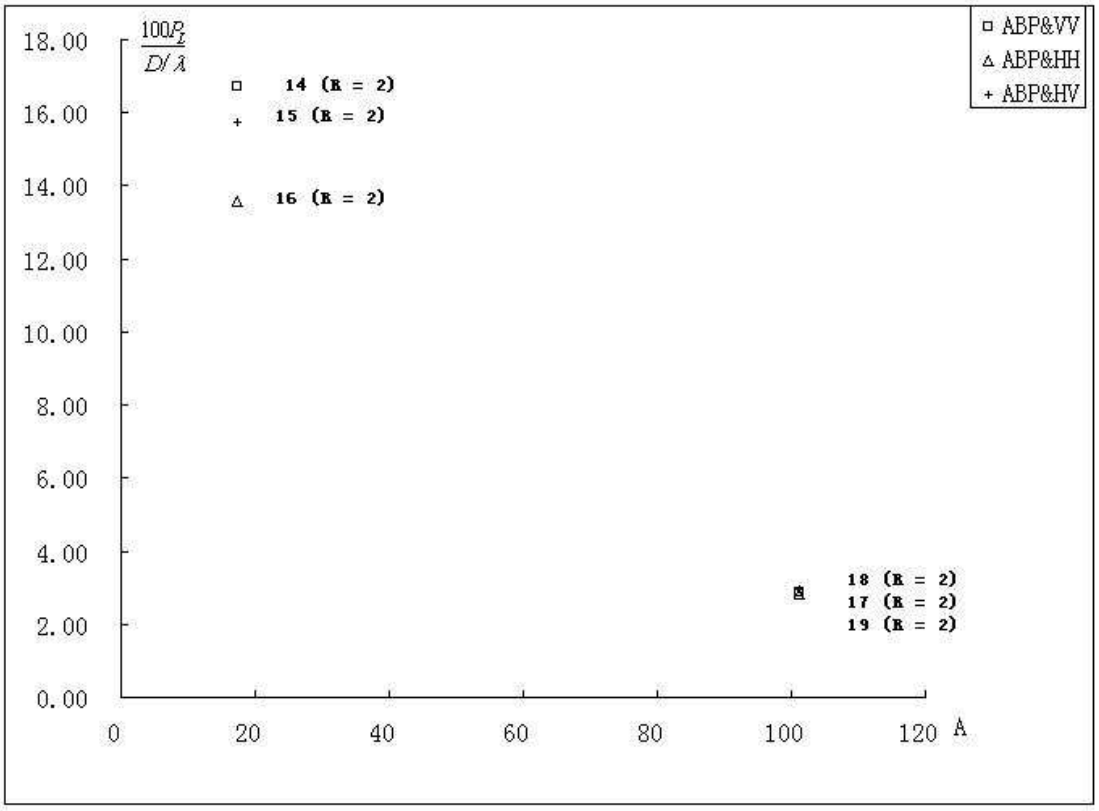

Observations:

- $\frac{P_L}{D/\lambda}$ for ABP is smaller than that for BBP by comparing Fig. 2-1-C and Fig. 2-1-D.
- $\frac{P_L}{D/\lambda}$ decreases with increasing A, by comparing data sets {#14, #17}, or {#15, #18}, or {#16, #19}.
- $\frac{P_L}{D/\lambda}$ decreases when the cross-sectional shape matches the linear polarization of electric field: data sets {#14, #16}, or {#17, #19}.
- Mismatching the linear polarization of electric field between transmitter and receiver can lead extra loss in $\frac{P_L}{D/\lambda}$: data sets {#15, #16}, or {#18, #19}.
- The effect of mismatching in the linear polarization of electric field between transmitter and receiver increases with increasing A: data sets {#14, #15}, and {#17, #18}

Figure 2-1-E: Brick tunnels

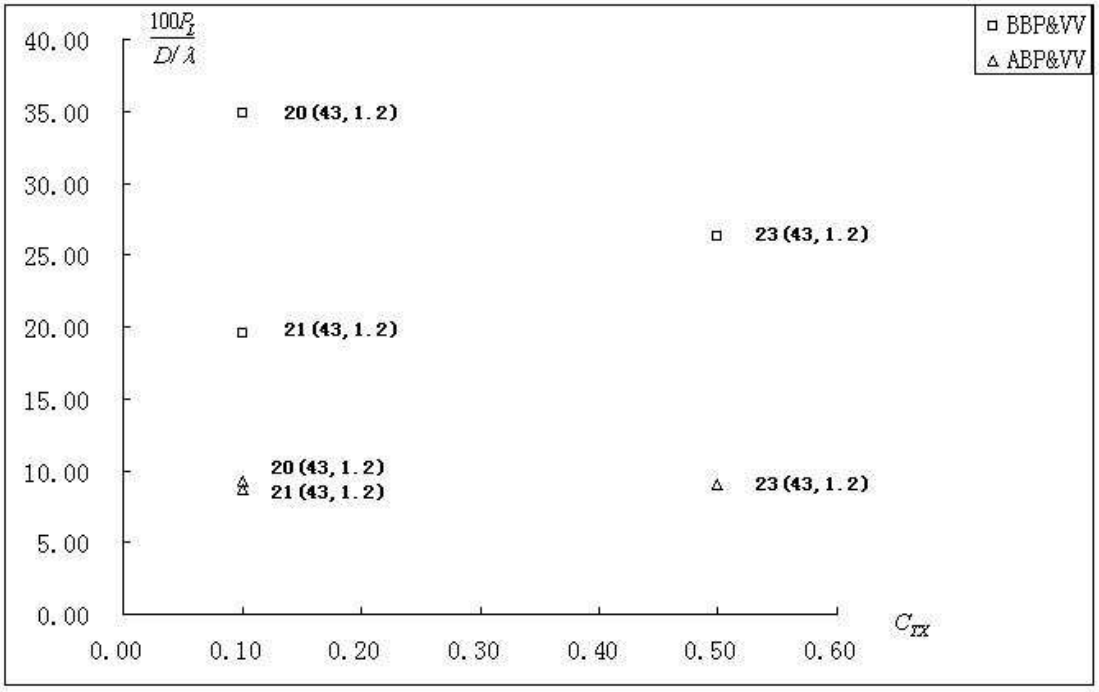

Observations:

- $\frac{P_L}{D/\lambda}$ for $C_{Tx} = 0.5$ is less than $\frac{P_L}{D/\lambda}$ for $C_{Tx} = 0.1$ from data sets {#20, #23},

  This agrees: $\frac{P_L}{D/\lambda}(C_{Tx} = 0.5) < \frac{P_L}{D/\lambda}(C_{Tx} \neq 0.5)$

- $\frac{P_L}{D/\lambda}$ for ABP is less than $\frac{P_L}{D/\lambda}$ for BBP. This agrees with [31].

- The reason why data sets {#20, #21} are so different is that although the C_{Tx} values are the same for these two data sets, the actual positions of transmitter in these two experiments are different. For data set #20, the position is at (0.1W, 0.7H) while (0.5W, 0.9H) for data set #21.

Figure 2-1-F: Bauxite tunnels

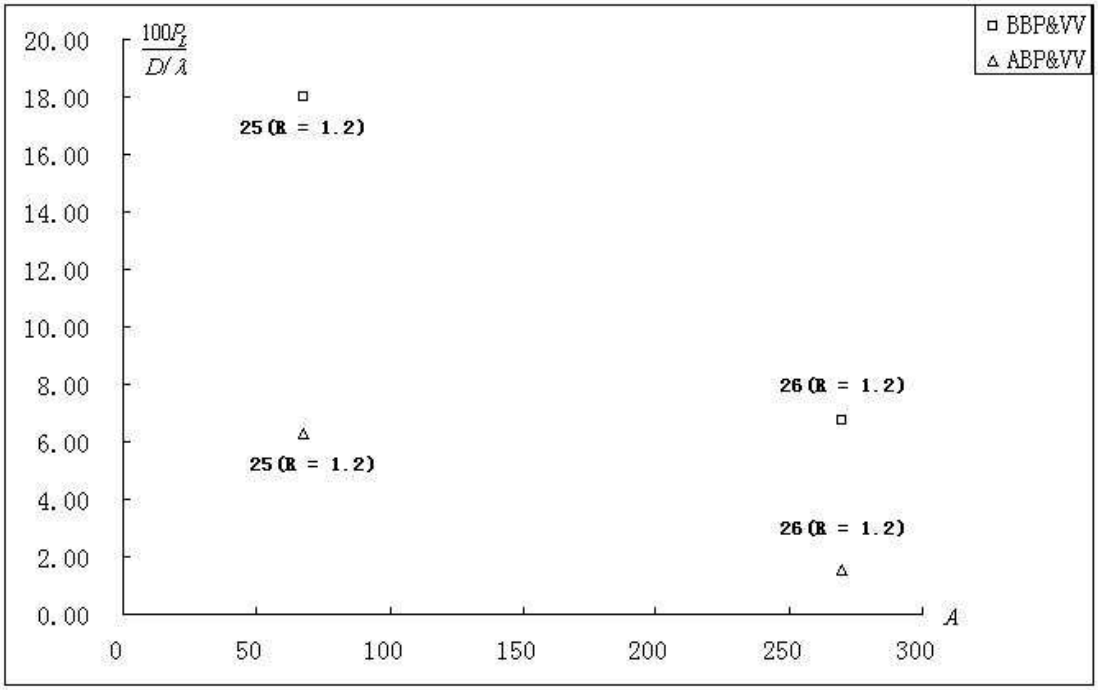

Observations:

- $\frac{P_L}{D/\lambda}$ decreases with increasing A from data sets {#25, #26}.
- $\frac{P_L}{D/\lambda}$ for ABP is less than that for BBP from data set #25 or data set #26.

Figure 2-1-G: Potash tunnels

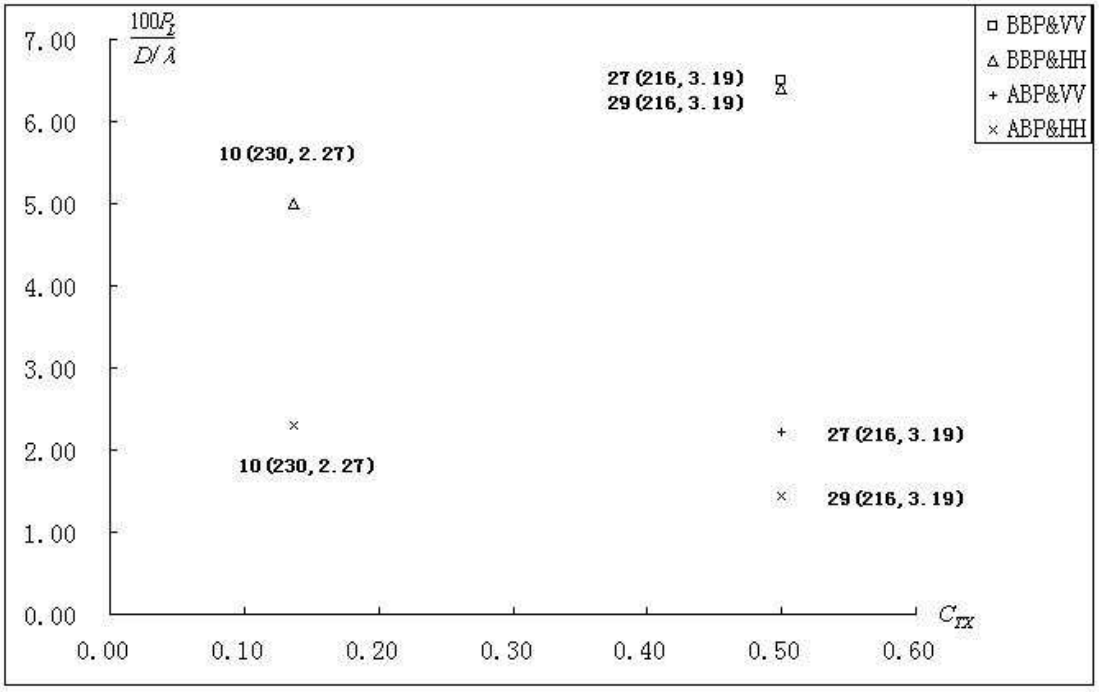

Observations:

- $\frac{P_L}{D/\lambda}$ decreases when the cross-sectional shape matches the linear polarization of electric field. This can be seen from data sets {#27, #29}. #29's horizontal polarization produces a smaller $\frac{P_L}{D/\lambda}$ than #27 in a tunnel, whose R is bigger than 1. This phenomenon is more obvious in ABP part than that in BBP part.
- $\frac{P_L}{D/\lambda}$ for ABP is less than that for BBP. This can be seen by comparing the values of BBP with those of ABP.
- In BBP part, data set #10's larger A overrides its smaller R and less favorable C_{Tx}, so its $\frac{P_L}{D/\lambda}$ is smaller than that for data set #29, but in ABP part, #29 has a smaller $\frac{P_L}{D/\lambda}$ than that for #10. As mentioned in Fig. 2-1-B, the effect of R is weakened in ABP part, so the reason why #29's $\frac{P_L}{D/\lambda}$ becomes smaller is the favorable C_{Tx}. Hence, the current author has a conclusion: in BBP part, since signal's fluctuation is mainly due to the reflection and refraction, A is the dominant factor for signal's transmission, the effect of other factors can be attenuated by enlarging A; While in ABP part, since LOS signal dominates the transmission and the reflection does not affect as much as in BBP, C_{Tx} and C_{Rx}

become the dominant factor. The signal would have the smallest $\frac{P_L}{D/\lambda}$ if $C_{Tx} = 0.5 \text{ and } C_{Rx} = 0.5$. This because in the central place of a tunnel, LOS signal receives the least interference.

2.2 Straight, Curved-Circle-Empty Tunnels

Figure 2-2: Straight, curved-circle-empty tunnels

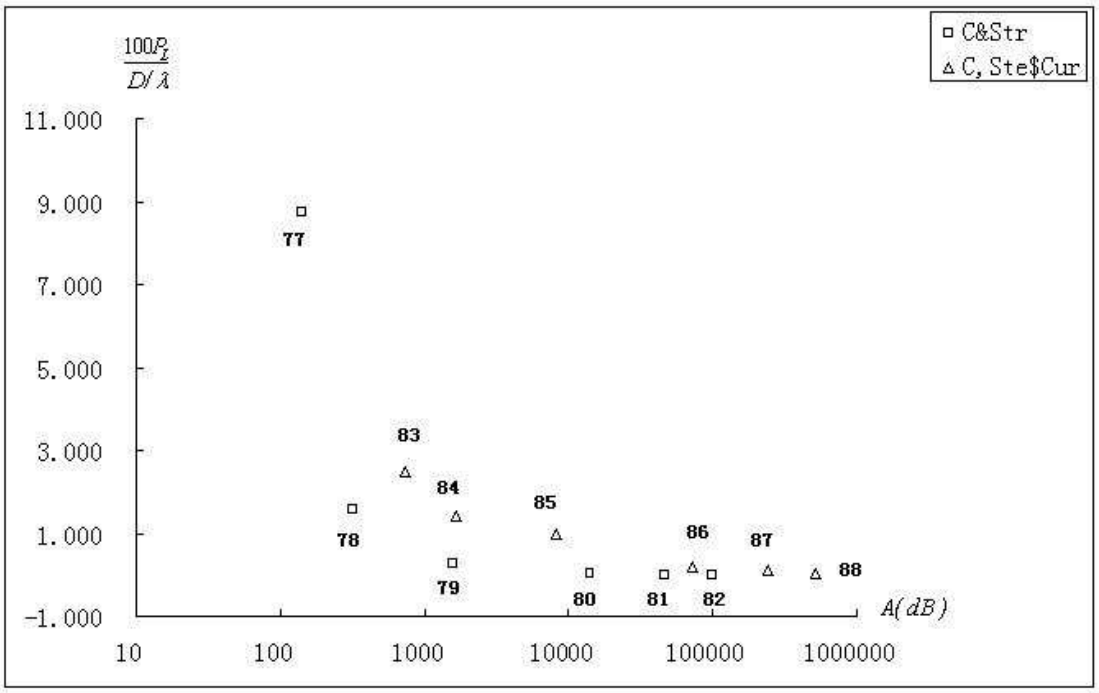

Observations:

- $\frac{P_L}{D/\lambda}$ decreases with increasing A
- Curved tunnel has bigger $\frac{P_L}{D/\lambda}$ than that for straight tunnel, due to curvature loss [20].

2.3 Straight-Arched-Empty Tunnels

Figure 2-3-A: Road tunnels with the same C_{Rx} and C_{Tx} and R bigger than 1

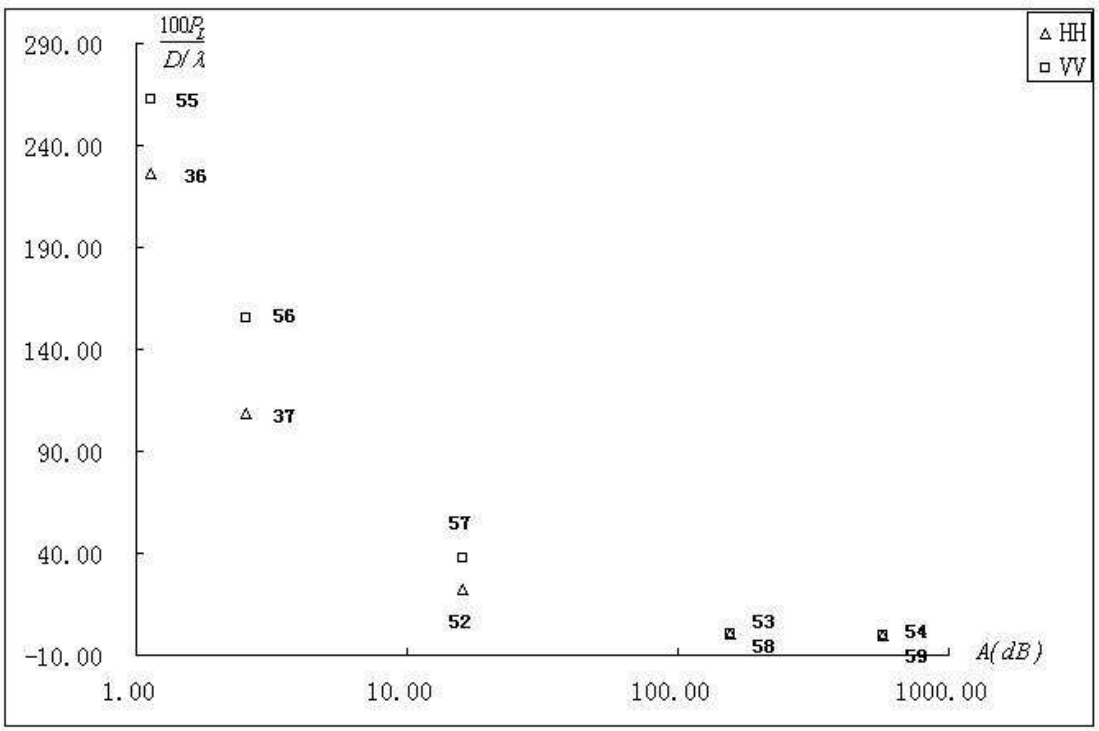

Observations:

- $\frac{P_L}{D/\lambda}$ decreases with increasing A.
- $\frac{P_L}{D/\lambda}$ decreases when the cross-sectional shape matches the linear polarization of electric field. This can be seen from data sets {#55, #36}, {#56, #37}, {#57, #52}. The horizontally polarized signal has a smaller $\frac{P_L}{D/\lambda}$ than vertically polarized in tunnels with R bigger than 1.
- Increasing A can attenuate the effect of reflection thus the effect of different polarization. This can be seen from data sets {#53, #58}, {#54, #59}.

Figure 2-3-B: Road tunnels with the same C_{Rx} and C_{Tx} and R bigger than 1

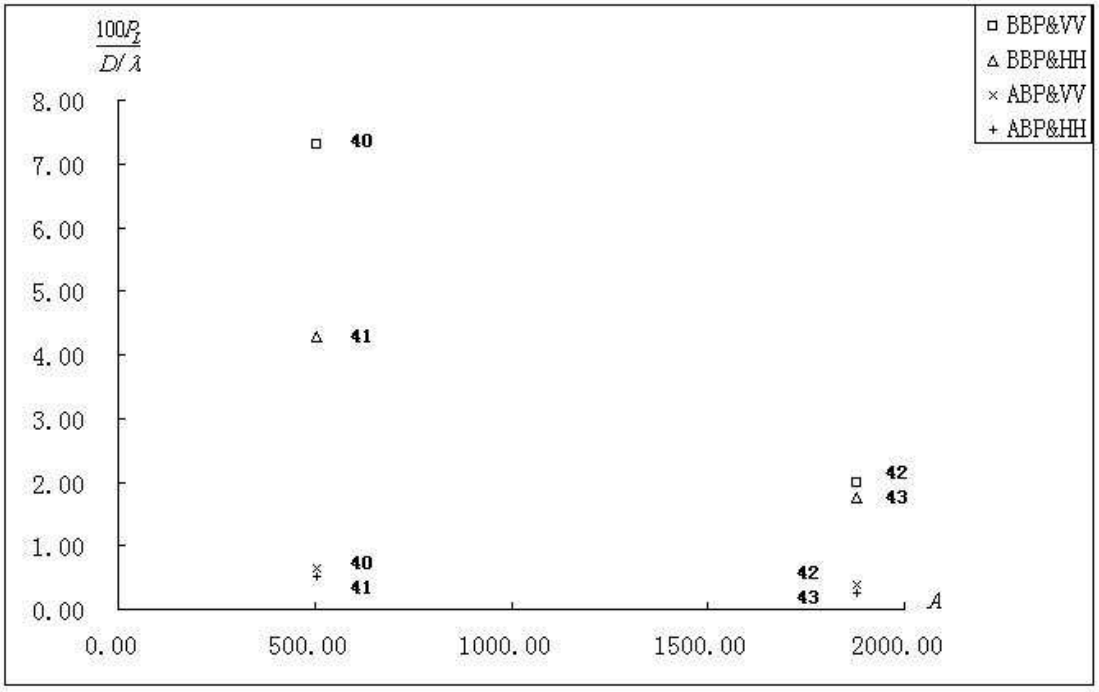

Observations:

- $\frac{P_L}{D/\lambda}$ decreases with increasing A.
- $\frac{P_L}{D/\lambda}$ for BBP is larger than that for ABP.
- $\frac{P_L}{D/\lambda}$ decreases when the cross-sectional shape matches the linear polarization of electric field. This can be seen from data sets {#40, #41}, {#42, #43}. The horizontally polarized signal has a smaller $\frac{P_L}{D/\lambda}$ than vertically polarized in tunnels with R bigger than 1.
- For BBP part, increasing A can attenuate the effect of different polarization. This can be seen from data sets {#40, #41, #42, #43}. The difference in $\frac{P_L}{D/\lambda}$ between vertical and horizontal polarization becomes small when A increases. But, this phenomenon is not detectable in ABP part. This because in BBP part, reflected signals and LOS signal are equally important while LOS signal dominates the ABP part, so A is a more important factor in BBP part than in ABP part.

2.4 Straight-Arched-Empty, Obstacle Tunnels

Figure 2-4: Coal mine tunnels

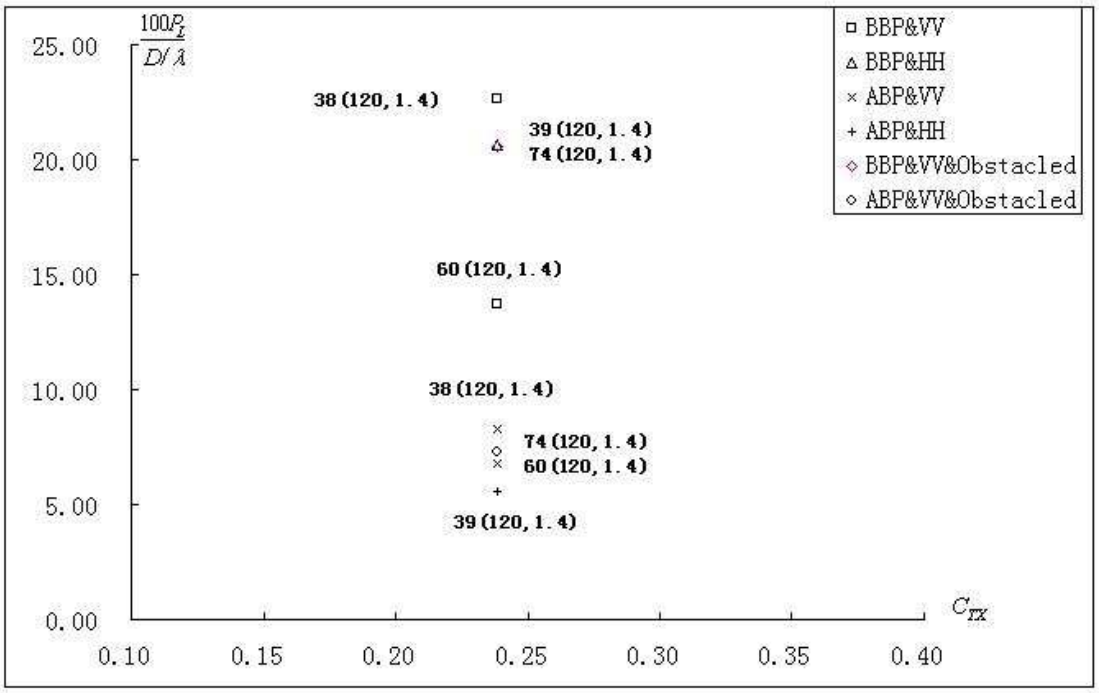

Observations:

- Data sets {#38, #39} are from one tunnel while {#60, #74} are from another tunnel. For data set #74, the tunnel is not empty: 20 cascaded trolleys (1.5 meters high, 1 meter wide, 3 meters long) stationed at 60 to 102 meters. Due to the difference of inner structure of these two tunnels, only the data sets from the same tunnel are comparable.
- $\frac{P_L}{D/\lambda}$ decreases when the cross-sectional shape matches the linear polarization of electric field. This can be seen from data sets {#38, #39}. The horizontally polarized signal has a smaller $\frac{P_L}{D/\lambda}$ than vertically polarized in tunnels with R bigger than 1.
- Obstacles in tunnels can lead a larger $\frac{P_L}{D/\lambda}$ than that in empty tunnels: data sets {#60, #74}. This can be explained as follows. The existence of these trolleys blocks some of the propagation paths and causes an additional propagation loss [31] thus a larger $\frac{P_L}{D/\lambda}$ compared with empty tunnels.

2.5 Straight, Curved-Arched-Empty Tunnels

Figure 2-5: Railway tunnels

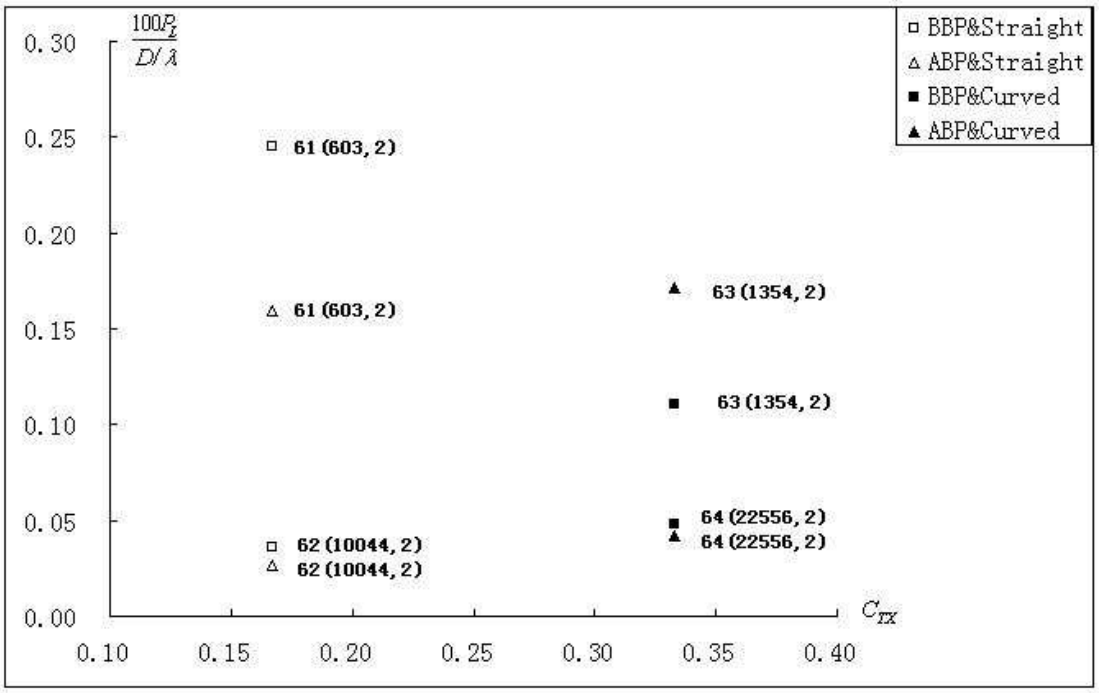

Observations:

- Data sets {#63, #64} are from a curved tunnel, which is rectilinear for the first 2 km and then exhibits a series of bends.
- $\frac{P_L}{D/\lambda}$ decreases with increasing A: data sets {#61, #62}, {#63, #64}.
- $\frac{P_L}{D/\lambda}$ for BBP is larger than that for ABP: #61, #62, and #64.
- Curvance can lead extra propagation loss thus a larger $\frac{P_L}{D/\lambda}$: {#62, #64}, the ABP part of {#61, #63}. #63 and #64's larger A and favorable C_{Tx} would cause smaller $\frac{P_L}{D/\lambda}$ but for the curvance.
- The curvance, after which no LOS signal exists, will increase $\frac{P_L}{D/\lambda}$ a lot. This can be seen from data sets #63. The curvance occurs in the ABP part of tunnel and leads no LOS signal for this part, so $\frac{P_L}{D/\lambda}$ increases and it is even bigger than its counterpart for BBP. This can be explained as follows: In ABP part, the signal's power is mainly from LOS component, no LOS signal means a huge power loss thus lead a very larger $\frac{P_L}{D/\lambda}$.

2.6 Branch-Rectangular-Empty Tunnels

Figure 2-6: Coal mine tunnels

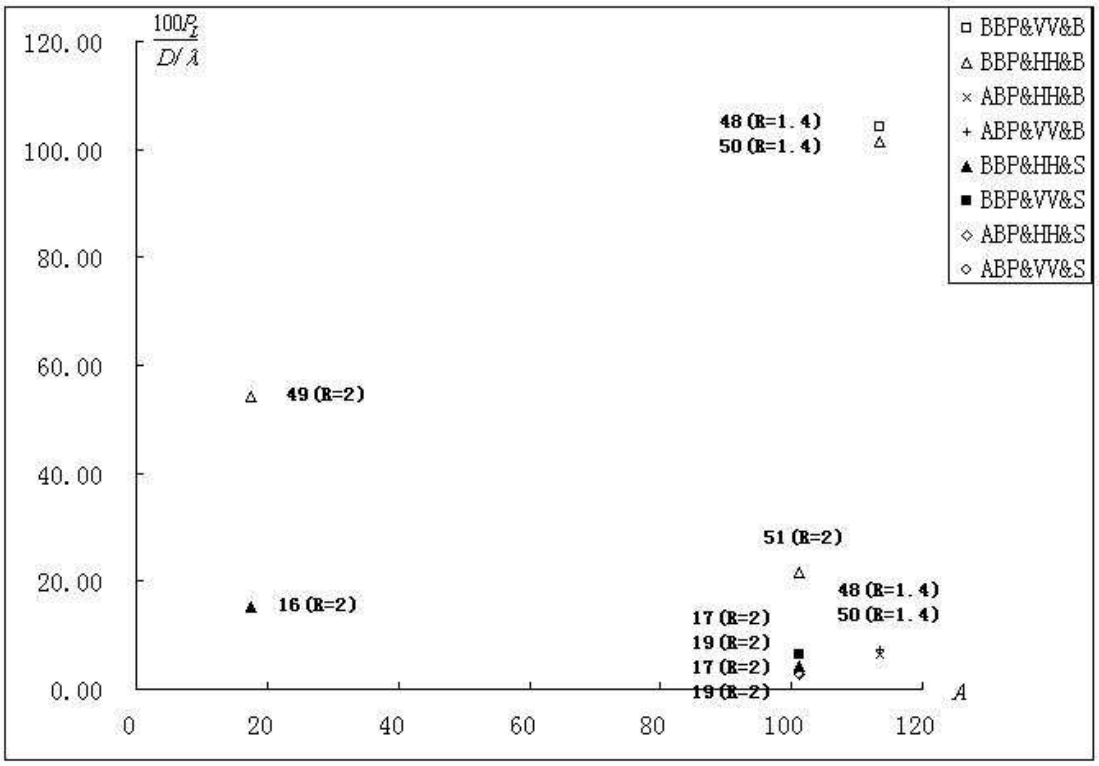

Observations:

- Data sets {#48, #50} are from a branched tunnel. The transmitter was in the branch tunnel, 10 m away from the junction formed by the branch and the main tunnel at an angle of 15 degrees. The receiver was being moved from the branch tunnel into the main one. Data sets {#49, #51} are from another branched tunnel. There was a corner along the propagation path. Due to the inner structure difference, only data sets coming from the same tunnel are comparable.
- $\frac{P_L}{D/\lambda}$ decreases with increasing A: data sets {#49, #51}.
- $\frac{P_L}{D/\lambda}$ for BBP is larger than that for ABP: data sets #48, #50.
- $\frac{P_L}{D/\lambda}$ decreases when the cross-sectional shape matches the linear polarization of electric field. This can be seen from data sets {#48, #50}. The horizontally polarized signal has a smaller $\frac{P_L}{D/\lambda}$ than vertically polarized in tunnels with R bigger than 1.
- For the two branched tunnels discussed above, LOS signal disappears in the BBP region, causing a big power loss, so $\frac{P_L}{D/\lambda}$ of BBP for the branched tunnels is bigger than that for the straight tunnels: data sets {#49, #16}, {#51, #19},{#50, #19}, {#48, #17}

- $\frac{P_L}{D/\lambda}$ of ABP for the branched tunnel is bigger than that for the straight tunnel: {#48, #17}, {#50, #19}. This can be explained as follows. As the receiver moved from the branch tunnel into the main one in a close distance from the transmitter, the distance for the break point to appear is shortened, so the ABP region for this branched tunnel is not as far as that for the straight tunnel and the reflected components are not attenuated as much as those in straight tunnels. This will cause a large fluctuation in the ABP region, although no LOS signal, and so a bigger $\frac{P_L}{D/\lambda}$ for this branched tunnel compared with the straight tunnel.

2.7 Underground Street

Figure 2-7: Underground street

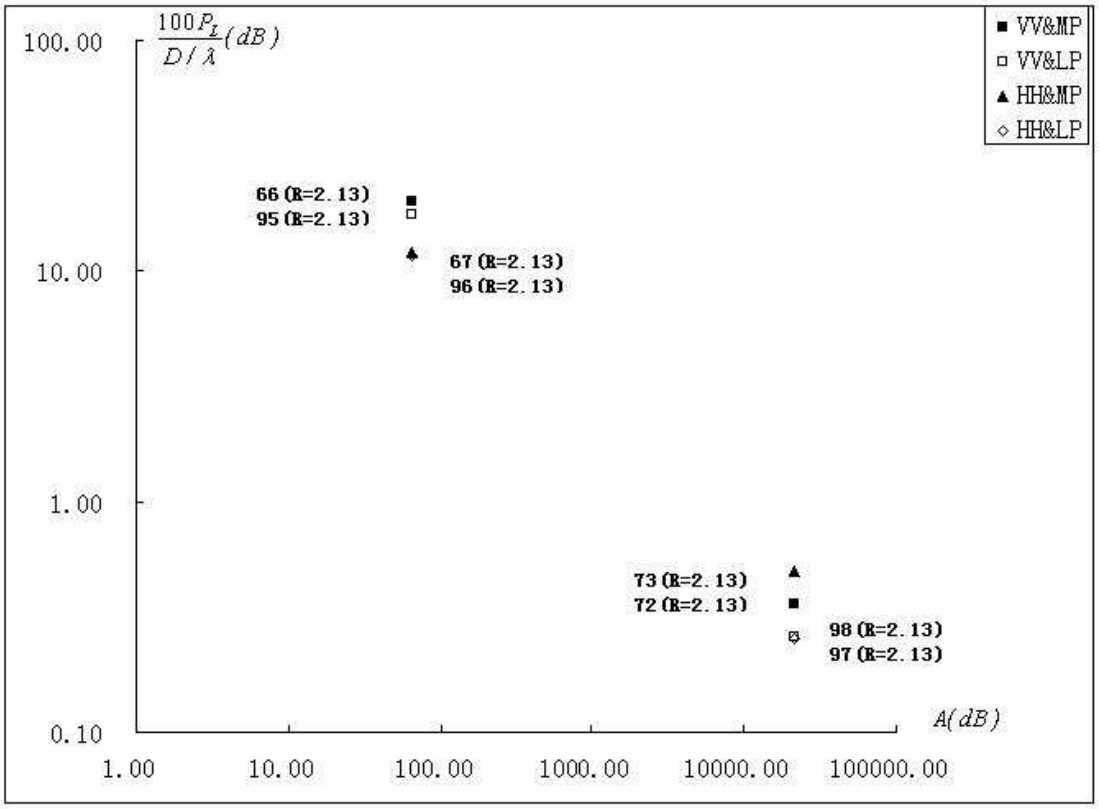

Observations:

- $\frac{P_L}{D/\lambda}$ for less pedestrians is less than that for more pedestrians: {#95, #66}, {#96, #67}, {#97, #72}, {#98, #73}. This is because pedestrians cause additional power loss. The effect of pedestrians increases as A increasing. [22] says that pedestrians act as a lossy dielectric component of rectangular waveguide below 5-6 GHz, and act as highly lossy obstacles for radio propagation above 6-7 GHz.
- $\frac{P_L}{D/\lambda}$ decreases with increasing A.
- $\frac{P_L}{D/\lambda}$ decreases when the cross-sectional shape matches the linear polarization of electric field. This can be seen from data sets {#95, #96}, {#66, #67}. The horizontally polarized signal has a smaller $\frac{P_L}{D/\lambda}$ than vertically polarized in tunnels with R bigger than 1.
- As A increasing, the effect of polarization difference decreases: data sets {#98, #97}, {#72, #73}. For these data sets, A is really large, so $\frac{P_L}{D/\lambda}$ for horizontal polarization is not smaller than that for vertical polarization any more.

2.8 Straight-Rectangular-Arched Tunnels

Figure 2-8-A: BBP part of concrete tunnels

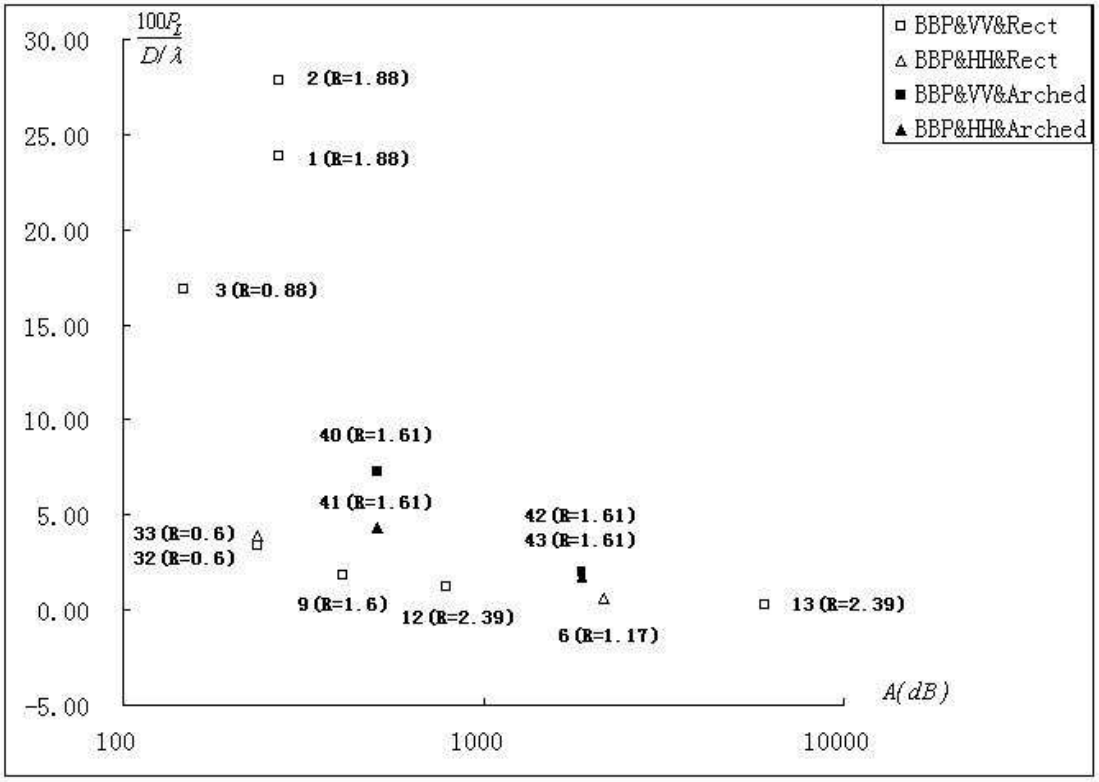

Observations:

- $\frac{P_L}{D/\lambda}$ for arched cross-sectional shape is larger than that for rectangular cross-sectional shape: data sets {#40, #9}. #40's larger A would have a smaller $\frac{P_L}{D/\lambda}$ than that for \#9, but for its arched cross-sectional shape. {#33, #41}, {#9, #41}, {#9, #42}, {#12, #42}, or {#12, #43} agree with this conclusion.

Figure 2-8-B: ABP part of concrete tunnels

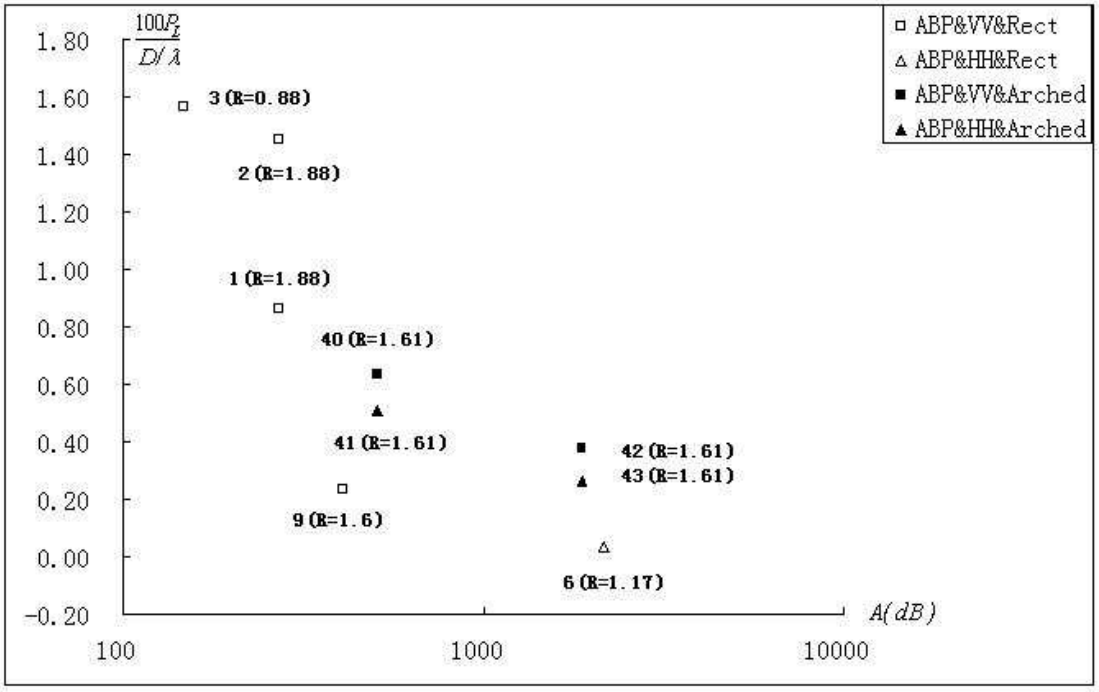

Observations:

- $\frac{P_L}{D/\lambda}$ for arched cross-sectional shape is larger than that for rectangular cross-sectional shape: {#40, #9}, {#41, #9}, {#42, #9}, or {#43, #9}.
- The effect of polarization is decreased in the ABP part compared with BBP part: in Fig. 2-8-A, $\frac{P_L}{D/\lambda}$ of #43 is smaller that of #9 due to #43's horizontal polarization and the tunnel's R, which is larger than 1. But in Fig. 2-8-B, there is a reverse result. This is because in ABP, the reflected components are not as important as in BBP, so the decreasing of $\frac{P_L}{D/\lambda}$ due to favorable polarization becomes small.

Figure 2-8-C: BBP part of coal mine tunnels

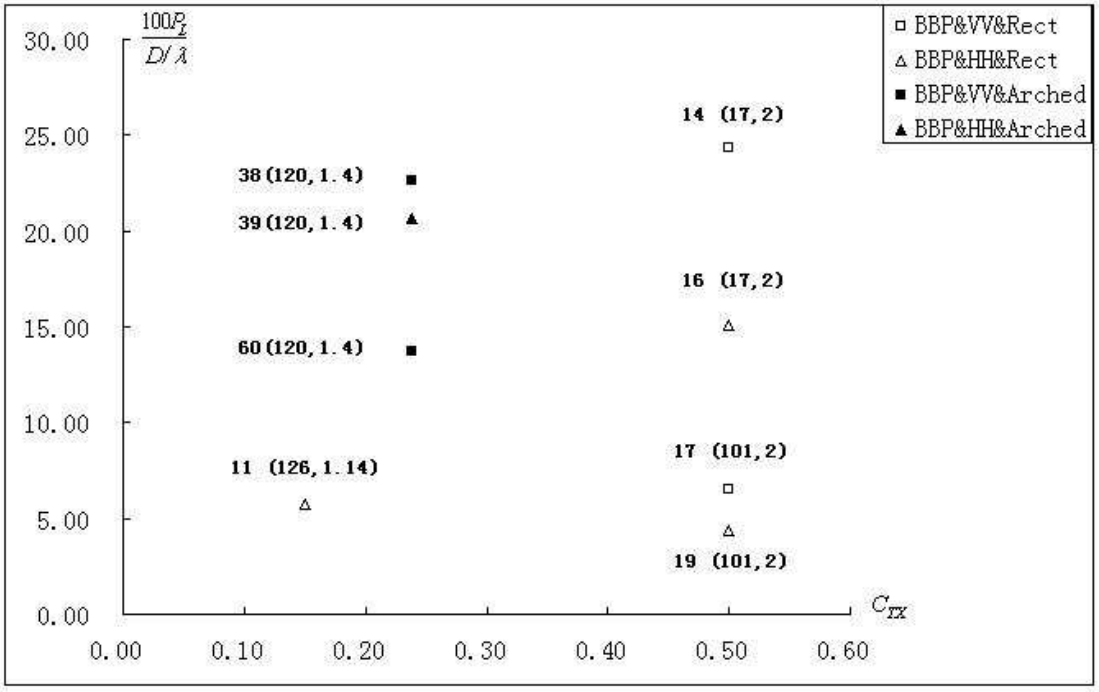

Observations:

- $\frac{P_L}{D/\lambda}$ for arched cross-sectional shape is larger than that for rectangular cross-sectional shape: {#17, #38}, {#17, #60}, {#16, #39}.

Figure 2-8-D: ABP part of coal mine tunnels

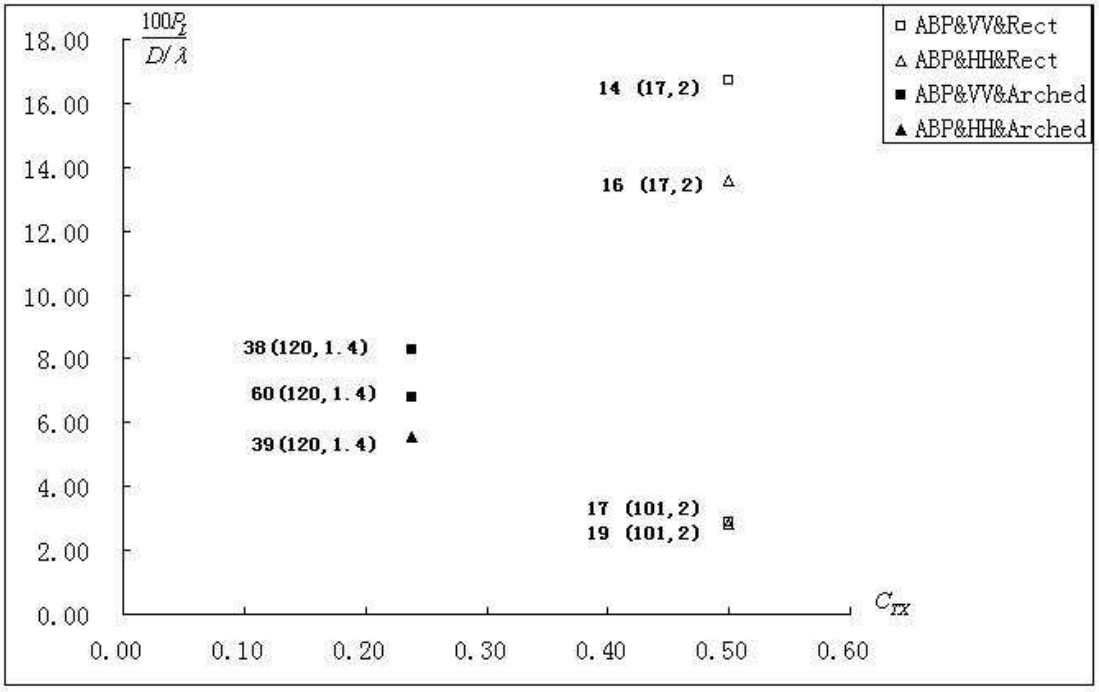

Observations:

- $\frac{P_L}{D/\lambda}$ for arched cross-sectional shape is larger than that for rectangular cross-sectional shape: {#17, #60}, {#17, #38}, {#19, #39}.
- Polarization for ABP is not as important as for BBP: in Fig. 2-8-C, $\frac{P_L}{D/\lambda}$ of #16 is smaller than that for #39 due to its bigger R, but this is not true in the ABP part, where #39's $\frac{P_L}{D/\lambda}$ is smaller than that for #16 due to its larger A.

2.9 Straight Tunnels with Different Wall Materials

Figure 2-9-A: BBP part of rectangular tunnels

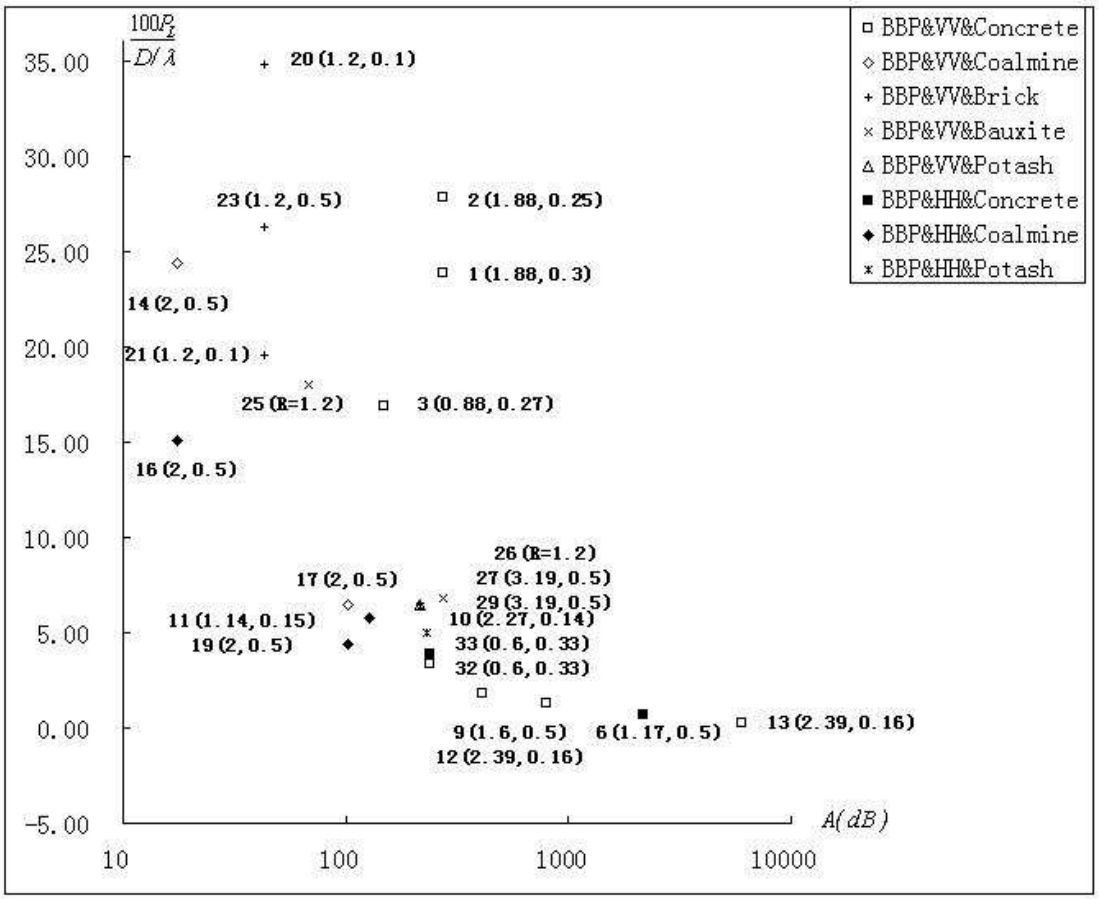

Observations:

- The data sets' structure is (R, C_{Tx}).
- $\frac{P_L}{D/\lambda}$ for brick tunnels is larger than that for coal mine tunnels: data sets {#14, #23}. #23's smaller R and larger A would have a smaller $\frac{P_L}{D/\lambda}$, but for the tunnel wall's material.
- $\frac{P_L}{D/\lambda}$ for potash tunnel is larger than that for coal mine tunnels: data sets {#11, #29}, or {#19, #29}. #29's larger R and A would have a smaller $\frac{P_L}{D/\lambda}$ but for its tunnel wall's material.
- $\frac{P_L}{D/\lambda}$ is inversely proportioned to the dielectric constant of tunnel walls. There are two physical constants for tunnel walls: conductivity(μ) and dielectric constant(ε). For potash tunnels, the common settings are μ = 6 and ε = 0.0001 s/m; for coal mine tunnels, μ = 10 and ε = 0.01 s/m. Because at frequencies above the VHF band, the surrounding material acts as a pure dielectric [8], the ohmic

loss related to μ is negligible and the refraction loss related to ε plays a dominant role in the attenuation. Only considering ε , potash tunnels with a smaller ε have a larger $\frac{P_L}{D/\lambda}$ than coal mine tunnels with a larger ε ; brick tunnels with ε = 4.5 have a larger $\frac{P_L}{D/\lambda}$ than coal mine tunnels.

Figure 2-9-B: ABP part of rectangular tunnels

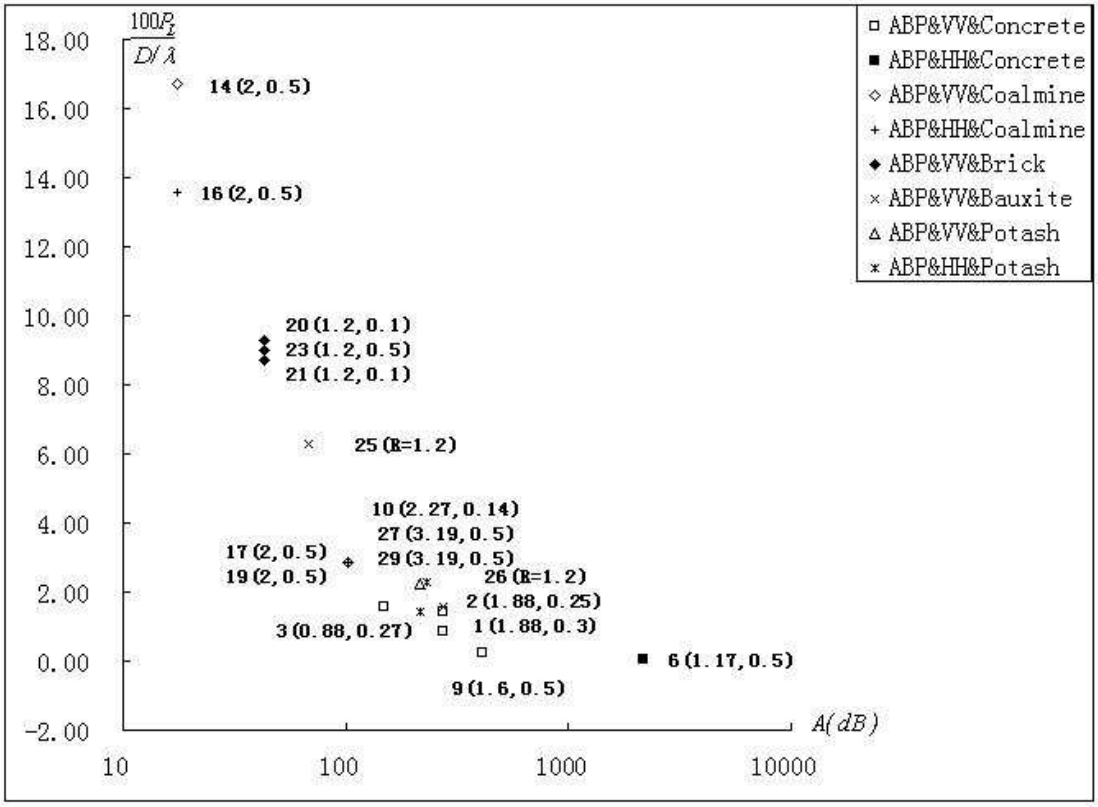

Observations:

- The data sets' structure is (R, C_{Tx}).
- No other conclusions.

Figure 2-9-C: BBP part of arched tunnels

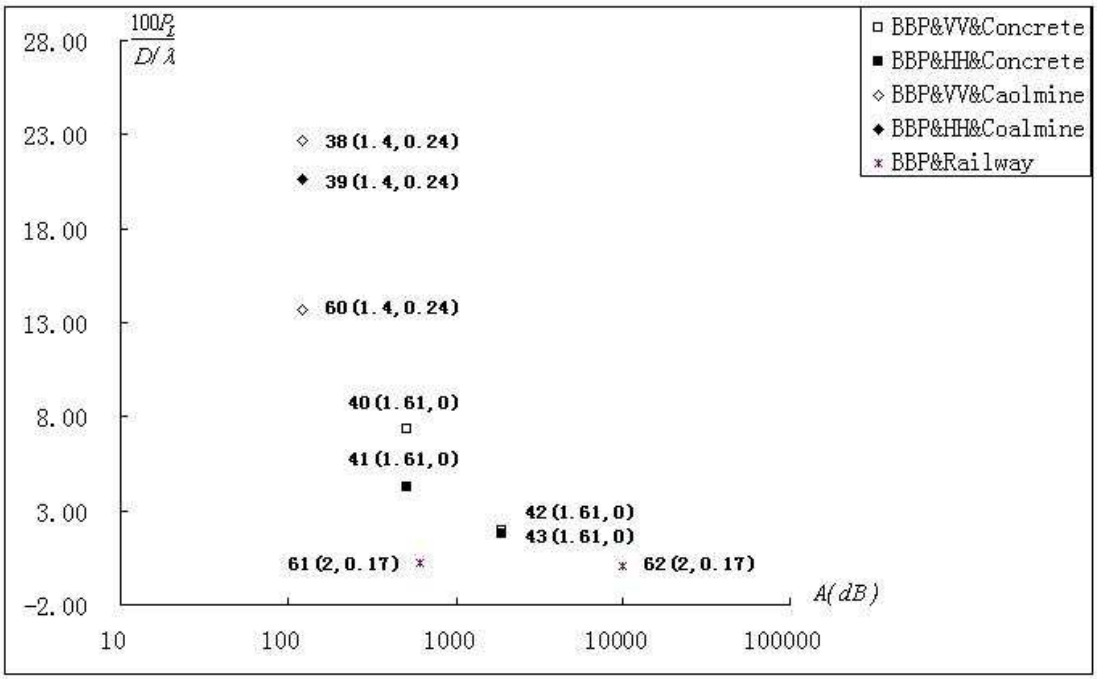

Observations:

- The data sets' structure is (R, C_{Tx}) and the polarization in railway tunnels is unknown.
- In BBP part of tunnel, $\frac{P_L}{D/\lambda}$ for railway tunnels is smaller than that for concrete tunnels: data sets {#61, #42}, or {#61, #43}. #61's smaller A would produce a larger $\frac{P_L}{D/\lambda}$ but for its tunnel material. The current author thinks that in a railway tunnel or subway tunnel, there are several things which do not exist in other tunnels, like rails on the floor and cables on the wall. These things go through the whole tunnels, acting like small wave guides and reflectors. So this can attenuate power loss thus produce a smaller $\frac{P_L}{D/\lambda}$. This agrees with [19] which avoids significant propagation loss by putting artificial reflectors on the walls.

Figure 2-9-D: ABP part of arched tunnels

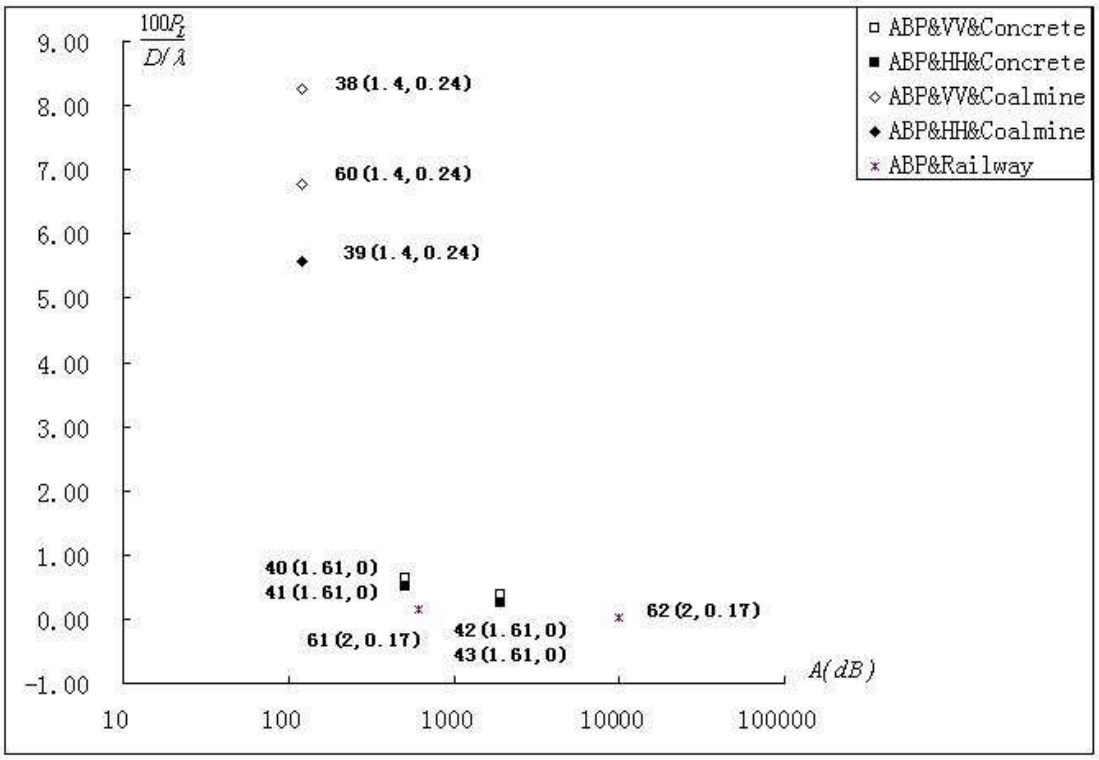

Observations:

- The data sets' structure is (R, C_{Tx}) and the polarization in railway tunnels is unknown.
- In ABP part of tunnel, $\frac{P_L}{D/\lambda}$ for railway tunnels is smaller than that for concrete tunnels: data sets {#61, #42}, or {#61, #43}.

2.10 α for Different Tunnels

Figure 2-10-A: Straight rectangular tunnels

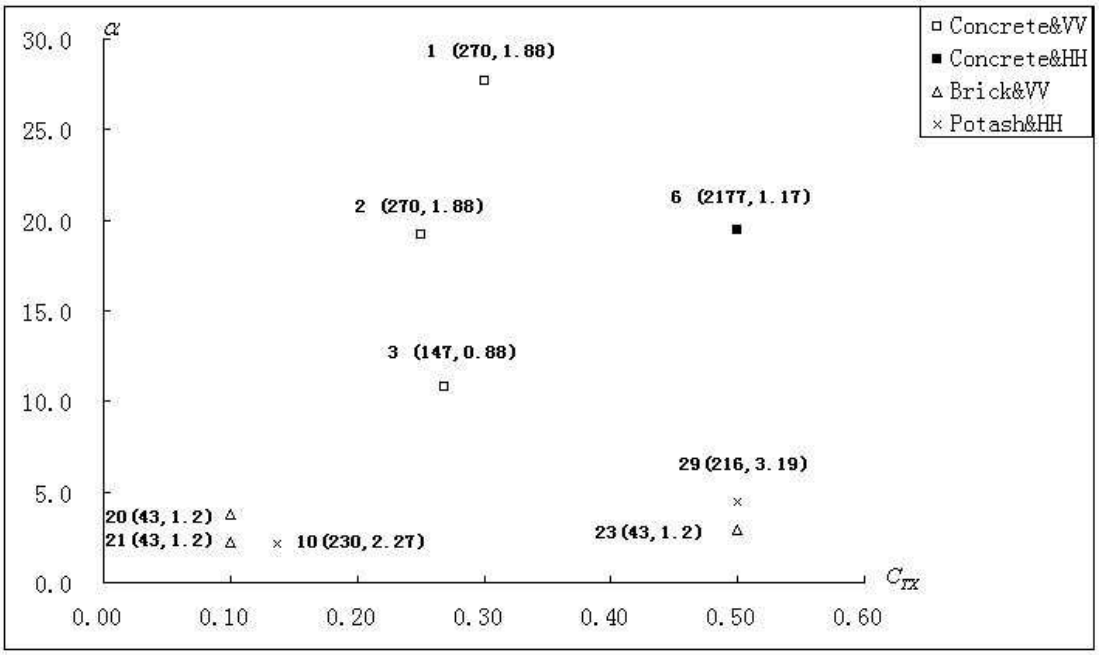

Observations:

- α increases as C_{Tx} is close to 0.5: data sets {#1, #2}. #1's C_{Tx} is closer to 0.5 than #2's, so its α is smaller. This can be explained as follows: in ABP part, C_{Tx} is the dominant factor for signal transmission. When $C_{Tx} = 0.5$, it will produce the smallest $\frac{P_L}{D/\lambda}$ for ABP part among all possible values for C_{Tx}, thus also lead a bigger α.
- Data sets {#10, #29} agree with the conclusion above. These two data sets have comparable A, and #29 has a larger α because its C_{Tx} equals 0.5.

Figure 2-10-B: Straight rectangular tunnels

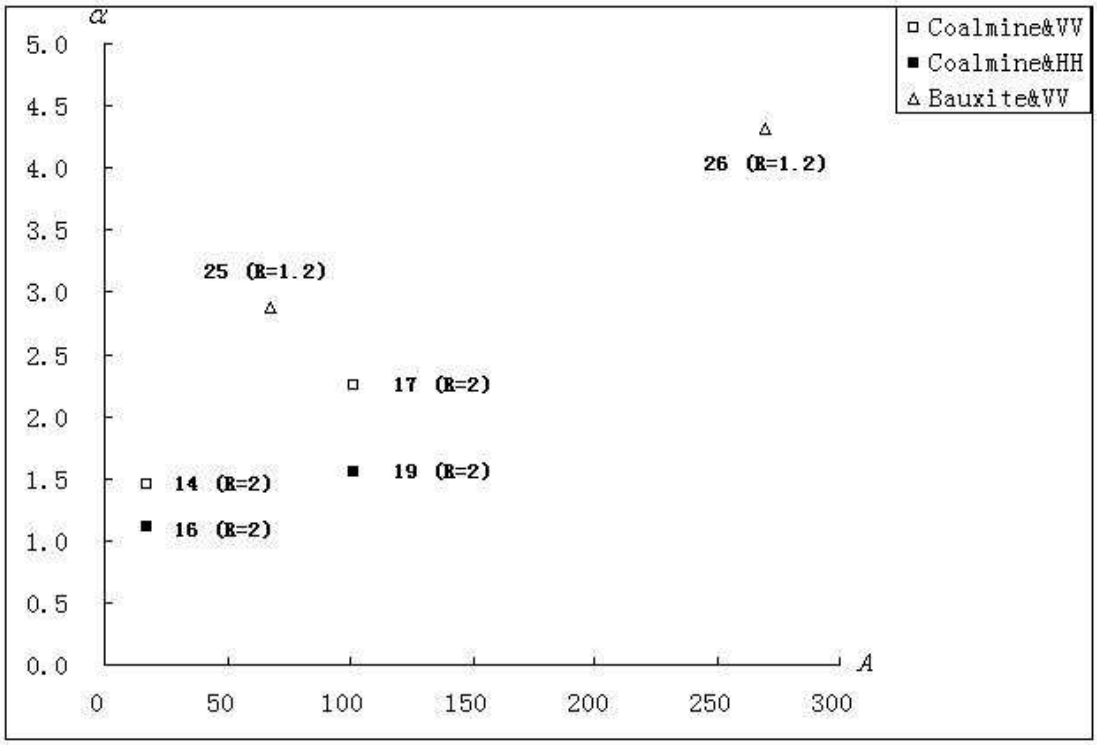

Observations:

- α increases as A increasing: data sets {#25, #26}, {#14, #17}, {#16, #19}.
- α decreases when the cross-sectional shape matches the linear polarization of electric field: {#14, #16}, {#17, #19}. This is because the matching will lead a smaller $\frac{P_L}{D/\lambda}$ for BBP part due to less reflections, thus have a smaller α.

Figure 2-10-C: Arched-empty, obstructed tunnels

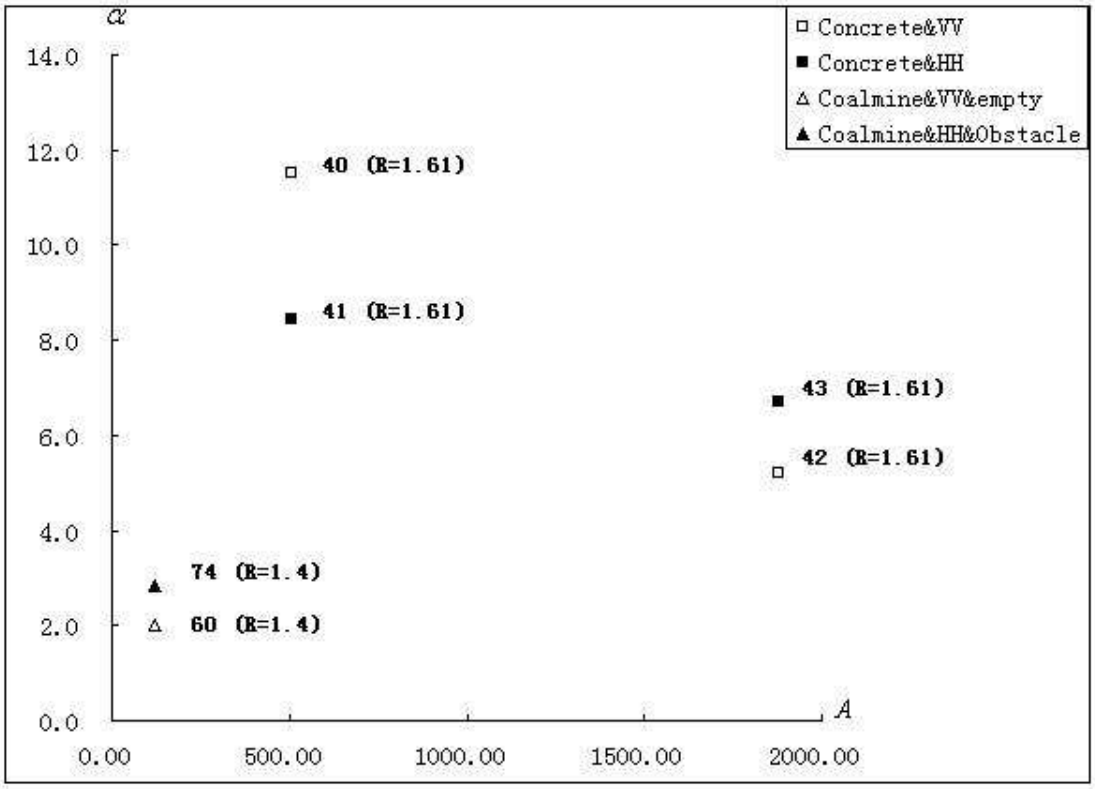

Observations:

- α decreases as A increasing: data sets {#40, #42\}, {#41, #43}. Combined with the conclusion in the Fig. 2-10-B, the relation between α and A is not linear.
- α for a obstructed tunnel is larger then than for an empty tunnel: {#74, #60}.

Figure 2-10-D: Straight, branched-empty coal mine tunnels

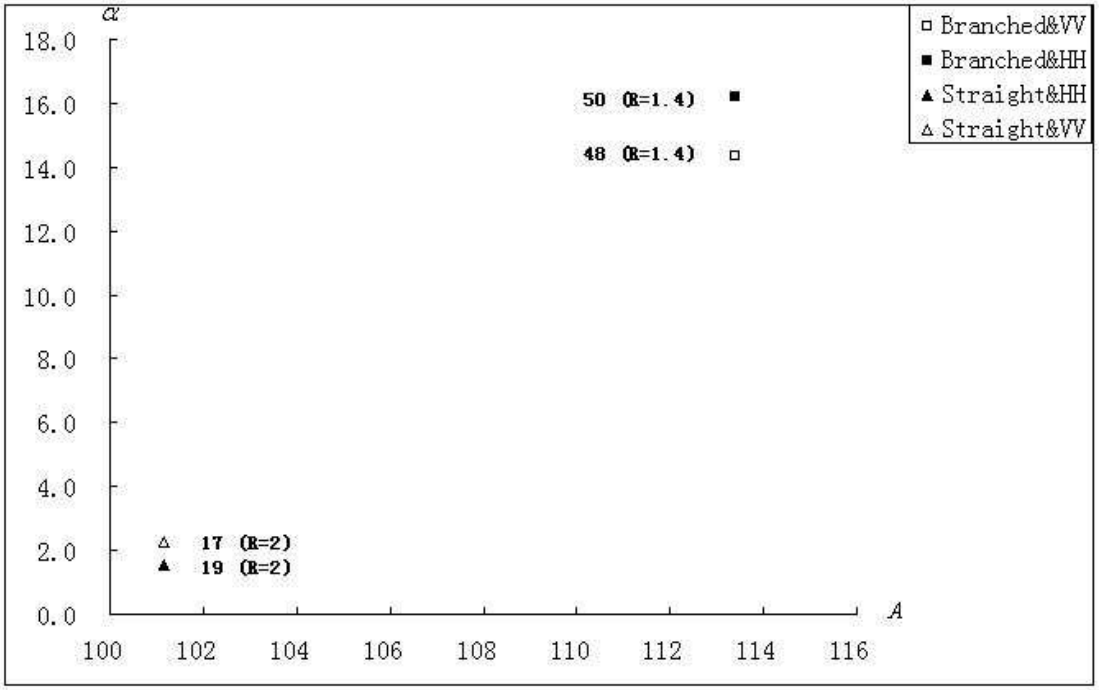

Observations:

- For the branched tunnel: the transmitter positioned in the branch was 10 m away from the junction formed by the branch and the main tunnel at an angle of 15 degrees. The receiver was being moved from the branch into the main one.
- α for branched tunnel is larger than that for straight tunnels: data sets {#50, #19}, {#48, #17}.

Chapter 3

Conclusions: One Independent Parameter Differs

3.1 A

- {#12, #13}: $100\frac{P_L}{D/\lambda}(BBP)$ decreases with increasing A. This agrees with the empirical trend by [20], which says $\frac{P_L}{D/\lambda}$ decreases with decreasing wavelength.
- {#14, #17}, {#15, #18}, and {#16, #19}: $100\frac{P_L}{D/\lambda}(BBP)$ and $100\frac{P_L}{D/\lambda}(ABP)$ decrease as A increasing. α increases as A increasing. Break point's longitudinal position increasing as A increasing. This is because as A increasing, it will take a longer distance for LOS signal becomes dominant over the reflected signals. In [41], it says "The larger the dimension is, the further the location of the break point is away from the transmitting antenna. This is the result of a larger cross-sectional tunnel being closer to a free space." In this paper, it models BBP region as free space and ABP region as a waveguide.
- A is the most important factor for break point's longitudinal position. The larger A, the further distance for break point to show up like the observation above. When A is small(hundreds wavelength), C_{Tx} does not affect break point's position too much, like data sets{#1, #2}, so does polarization like data sets {#14, #15, #16\}, {#17, #18, #19}, {#27, #29}, {#38, #39}, {#40, #41}; when A is big(thousands wavelength), these two factors will make some difference(hundreds wavelength) in break point's position, like data sets {#42, #43}. Matching between cross-sectional shape and linear polarization of electric field in #43 takes a longer distance to let LOS signal become dominant over reflected signals than #42.
- {#25, #26}: $\frac{P_L}{D/\lambda}$ for both BBP and ABP parts decreases with increasing A. α increases as increasing A.
- Data sets from #77 to #82: $\frac{P_L}{D/\lambda}$ decreases with increasing A.

- Data sets from #83 to #88: $\frac{P_L}{D/\lambda}$ decreases with increasing A.
- #36, #37, and from #52 to #54: $\frac{P_L}{D/\lambda}$ decreases with increasing A; data sets #55 to #59: $\frac{P_L}{D/\lambda}$ decreases with increasing A. This agrees with the observation found in [2], which says "The resulting attenuation is found to increase monotonically with the inverse of frequency".
- {#40, #43}, {#41, #43}: $100\frac{P_L}{D/\lambda}(BBP)$ and $100\frac{P_L}{D/\lambda}(ABP)$ decrease with increasing A.
- {#61, #62}, {#63, #64}: $100\frac{P_L}{D/\lambda}(BBP)$ and $100\frac{P_L}{D/\lambda}(ABP)$ decrease with increasing A$. Theoretical explanation in [42]: "A tunnel can be considered as a lossy waveguide and, since the walls are not infinitely conductive, hybrid modes $EM_{m,n}$ will be excited by the transmitting antenna. Using certain simplifying hypotheses, it can easily be demonstrated that path loss is a continually decreasing function of frequency".
- {#49, #51}: $100\frac{P_L}{D/\lambda}(BBP)$ decreases with increasing A.
- {#98, #97}, {#72, #73}: As A increasing, the effect of polarization difference decreases. For these data sets, A is really large, so $\frac{P_L}{D/\lambda}$ for horizontal polarization is not smaller than that for vertical polarization any more.
- Data sets {#66, #72}, {#95, #97}, {#67, #73}, {#96, #98}: $\frac{P_L}{D/\lambda}$ decreases with increasing A. The similar observation in [22]: "From the experimental results, the attenuation constant decreases with increasing frequency as a whole."

3.2 C_{Tx}

- {#1,#2}:$100\frac{P_L}{D/\lambda}(BBP)$ and $100\frac{P_L}{D/\lambda}(ABP)$ decreases with C_{Tx} approaching 0.5. α increases as C_{Tx} approaching 0.5.
- {#20, #23}: $\frac{P_L}{D/\lambda}$ for $C_{Tx}=0.5$ is less than $\frac{P_L}{D/\lambda}$ for $C_{Tx}=0.1$ for both BBP and ABP parts, this agrees: $\frac{P_L}{D/\lambda}(C_{Tx}=0.5)<\frac{P_L}{D/\lambda}(C_{Tx}\neq 0.5)$

3.3 Polarization

- {#32, #33}:$100\frac{P_L}{D/\lambda}(BBP)$decreases when the cross-sectional shape matches the linear polarization of electric field. In this case, $\frac{P_L}{D/\lambda}$ for VV is less than that for HH. [37] explained this trend as follows: The floor and the ceiling can be represented by a high dielectric constant or as conducting materials, in which case the reflection for both polarizations is high. The walls are better approximated as dielectric materials. The waves that have polarization perpendicular to the walls (horizontally polarized) undergo a Brewster angle phenomenon and penetrate the walls without any reflection at all. At angles near the Brewster angle the reflection is not zero but greatly reduced. No such effects are present for the vertical polarization (parallel to the walls).
- {#32, #33,#34,#35}: Mismatching the linear polarization of electric field between transmitter and receiver can produce extra loss in$100\frac{P_L}{D/\lambda}(BBP)$. #34 and #35, whose polarization is mismatched, have bigger $100\frac{P_L}{D/\lambda}(BBP)$ than that for the data sets #32 and #33, whose polarization is matched.
- {#33, #34}: The effect of mismatching in the linear polarization of electric field between transmitter and receiver becomes more important with a larger A. The transmitter in #33 sending horizontal signal, would have a bigger $100\frac{P_L}{D/\lambda}(BBP)$ than #34, which sends vertical signal, in a tunnel whose R is less than 1, but for the polarization mismatch between transmitter and receiver in #34 and the relatively big A.
- For {#14, #16}, {#17, #19}:$100\frac{P_L}{D/\lambda}(BBP)$ and $100\frac{P_L}{D/\lambda}(ABP)$ decrease when the cross-sectional shape matches the linear polarization of electric field. For {\#15, #16}, {#19, #18}: Mismatching the linear polarization of electric field between transmitter and receiver can lead extra loss in $100\frac{P_L}{D/\lambda}(BBP)$ and $100\frac{P_L}{D/\lambda}(ABP)$. From {#14, #15, #17, #18}: The effect of mismatching in the linear polarization of electric field between transmitter and receiver increases with increasing A. The polarization mismatching in #15 (HV) is not important compared with #14(VV), in a small tunnel, with R bigger than 1. The reason is that the signal attenuation in this small tunnel is mainly due to reflections and refractions so that the effect of mismatching in the linear polarization of electric field between transmitter and receiver is weakened. On the other hand, data sets #17 and #18 are in a big tunnel, so the attenuation due to reflections is decreased, hence, the polarization mismatching becomes important in this case.
- {#27, #29}: $\frac{P_L}{D/\lambda}$ for both BBP and ABP parts decreases as the cross-sectional shape matching the linear polarization of electric field, while α increases. [35]

found the similar trend "the rate of attenuation is smaller for horizontal polarization compared with vertical polarization".

- From data sets {#55, #36}, {#56, #37}, {#57, #52}: $\frac{P_L}{D/\lambda}$ decreases when the cross-sectional shape matches the linear polarization of electric field. From data sets {#53, #58}, {#54, #59}: Increasing A can attenuate the effect of reflection thus the effect of different polarization.
- {#40, #41}, {#42, #43}:$100\frac{P_L}{D/\lambda}(BBP)$and $100\frac{P_L}{D/\lambda}(ABP)$ decrease when the cross-sectional shape matches the linear polarization of electric field. For BBP part, increasing A can attenuate the effect of different polarization. This can be seen from data sets {#40, #41, #42, #43}. The difference in $100\frac{P_L}{D/\lambda}(BBP)$ between vertical and horizontal polarization becomes small when A increases. But, this phenomenon is not detectable in ABP part. This because in BBP part, reflected signals and LOS signal are equally important while LOS signal dominates the ABP part, so A is a more important factor in BBP part than in ABP part. α decreases as A increasing, combined with previous conclusion α increases as A increasing, the relation between α and A is not linear.
- {#38, #39}: $100\frac{P_L}{D/\lambda}(BBP)$ and $100\frac{P_L}{D/\lambda}(ABP)$ decrease when the cross-sectional shape matches the linear polarization of electric field.
- {#48, #50}: $100\frac{P_L}{D/\lambda}(BBP)$ and $100\frac{P_L}{D/\lambda}(ABP)$ decrease when the cross-sectional shape matches the linear polarization of electric field
- From data sets {#95, #96}, {#66, #67}, {#68, #69}: $\frac{P_L}{D/\lambda}$decreases when the cross-sectional shape matches the linear polarization of electric field.

3.4 Overall Conclusions

- Analysis of narrowband experimental data reveals that power distance factors[2] range form 1.87 to 4.49 with a standard deviation of 3.69-7.37. The effects of pedestrians, vehicles, and curvature cause extra losses from 6 to 30 dB. The slow variations of the received signals follow the lognormal distribution with averaged standard deviations of 4.7 dB for a 900-MHz channel. [20]
- Higher frequency signal has a smaller power distance factor. This is contrary to what has been found in other radio propagation environments.[20]
- The power distance factors at the frequency of 900 MHz for horizontally and vertically polarized signals showed an increase from 2.96 to 3.71 for the almost

[2] The signal power distance factor is defined by the gradient of the linearly fitted line to the local mean of the received signal in decibels versus distance from transmitter to receiver on a logarithmic scale [20]

emptied tunnel to 3.17-5.49 for fully occupied tunnel conditions. The measurements in the TCMH tunnel indicated a 13-dB shadowing loss at the frequency of 900 MHz caused by the coal mine train. The shadowing loss due to a car or a truck was measured in the TFH tunnel. The truck caused 6-10-dB additional loss while the car shadowing effects were negligible.[20]

- Tunnels curvature should yield more shadowing for the received signals in the out-of-sight region. Curvature extra loss around the junctions of the TCMH tunnel was measured by placing the transmitter in the middle of the branch tunnel and moving the receive antenna at half-tunnel height along route. An extra loss of 17 and 30 dB at 900 MHz was measured toward both the end at an obtuse angle and entry at an acute angle of the main tunnel, respectively. The investigation of the curvature extra loss due to the existence of a sharper penumbra region from the lit region to the shadow region. There was 9 dB more curvature extra loss at 1800 MHz with respect to 900 MHz in the NS 173 tunnel. Measurements of different polarized signals indicated that curvature loss was independent of polarization. [20]
- The propagation loss was insensitive to the location of the transmit antenna. Because of the dipole antenna used in the measurement, the antenna insertion loss was sensitive to the location.[20]
- The effects of pedestrians, vehicles, and curvature in tunnel environments on propagation were also investigated. The power distance factors for 900-MHz horizontally and vertically polarized signals were increased from 2.96 and 3.71 to 3.17 and 5.49 in an almost vacant to fully occupied underground market tunnel, respectively. Thus, pedestrians constituted an additional loss. The measurements in a coal-mine tunnel indicated that there was 13-dB shadowing loss at 900 MHz caused by the coal-mine train. The shadowing loss due to a car or truck was measured in a road tunnel with the truck causing a 6–10-dB additional loss and the car’s shadowing effect being negligible. In comparison with either pedestrian or vehicle extra loss, the tunnel curvature yielded much more shadowing loss. Depending upon the location of the receive antenna, whether it was in the penumbra or deep shadow region, the shadowing losses were measured from 17 and 30 dB around the junction of the coal-mine tunnel at 900 MHz. The frequency dependence of shadowing loss on frequency was studied in the NS 173 tunnel. There was 9 dB more extra loss at 1800 MHz with respect to that of 900 MHz. This was due to a sharper penumbra region. It was also found that the shadowing loss was approximately the same for the horizontal and vertical polarization. This observation was consistent with the theory of geometrical optics.[20]
- The model [41] yields more accurate locations of the break points for tunnel microcells. The formula for urban microcells in [11] is inapplicable for tunnel microcells.
- It is seen that the antenna position greatly affects the location of the break point. For instance, the location of the break point goes further as the transmitting antenna is closer to the tunnel ceiling. This is because the antenna closer to the

ceiling causes a larger coupling loss to the dominant waveguide mode; as a result, it takes a longer distance for the dominant mode to become stronger.[41]

- The location of the break point is highly related with the tunnel-transversal dimension. The larger the dimension is, the further the location of the break point is away from the transmitting antenna. This is the result of a larger cross-sectional tunnel being closer to a free space. In addition, it is found that the antenna gain has no effect on the location of the break point in the tunnel.[41]
- A large loss in signal strength occurs when the receiving antenna is moved around a corner into a cross tunnel; and that the signal strength around the corner is independent of receiving antenna orientation. [1]
- The reason that path loss exponent is high in an out-of-sight area is that there is no direct wave but only the reflected waves, which attenuates rapidly with distance due to multiple reflections. [15]
- The power roll off is better described by a distributed loss model $(e^{-\alpha d})$ than by $d^{-\gamma}$, the reverse for a room. [37]
- The field strength received in the lower position (Antenna 1) is larger than that received in the higher one (Antenna 2). This characteristic was common to the patterns for frequencies below 5-6 GHz. This phenomenon indicates that radio waves propagate easily in the region with pedestrians. [22]
- The most significant feature is that the maximum field strength occurs in the region with pedestrians for both polarized waves, as in Fig. 4. This phenomenon indicates that most of the energy travels in the region with pedestrians. [22]
- Conductivity increases and the dielectric constant decreases with frequency, with much lower variations for ε. [4]
- The propagation loss before the breakpoint is 28 dB over the distance of 42 m, which is very close to that in the empty trolley passageway. The propagation loss after the breakpoint is found to increase by 5.8 dB/100 m as compared with that in the empty trolley passageway. Since both trolley and belt passageways have almost the same tunnel structure, the propagation loss due to the tunnel itself should be very close. Thus it is believed that the increased 5.8 dB/100 m loss is caused by the belt conveyor itself. [31]
- The additional loss is related to the sharpness of bents and the cross-sectional area ratio of long wall coal mining equipment to their operational spaces. the additional loss is 5 dB due to a 175° bent and increases to 25 dB for a 90° bent. The maximum additional loss due to obstruction by common long wall coal mining equipment is 25 dB, which occurs when two trains of trolleys are in parallel. [31]
- The propagation was shown to be insensitive to the shape of cross section [15]. The arched tunnel can be treated as an equivalent rectangular tunnel. The equivalent width is set to be equal to the width of the original arched tunnel, while the height can thus be obtained by assuming that the equivalent tunnel has the same cross section as the original arched tunnel.[24]

- We found a surprising relation. There exists a "critical distance", $l_{crit} = \frac{d^2}{\lambda}$ where d is the largest cross dimension and λ the free-space wavelength. It specifies a minimum distance from the source, either an antenna in the tunnel or the tunnel entrance aperture, where almost all higher loss modes have disappeared. The median power level at that position can serve as the basis for coverage length prediction in the tunnel. [13]
- One factor accounts for losses due to roughness of the tunnel wall which will tend to defocus the rays traveling down the tunnel.[9]

3.5 Obstacles

- {#60, #74}: Obstacles in tunnels can lead a larger $100\frac{P_L}{D/\lambda}(BBP)$ and $100\frac{P_L}{D/\lambda}(ABP)$ than that in empty tunnels. This can be explained as follows. In [31], "The existence of these trolleys blocks some of the propagation paths and causes an additional propagation loss" thus a larger $100\frac{P_L}{D/\lambda}(BBP)$ and $100\frac{P_L}{D/\lambda}(ABP)$ compared with empty tunnels. α for obstructed tunnel is bigger than that for empty tunnels.
- {#95, #66}, {#96, #67}, {#97, #72}, {#98, #73}: $\frac{P_L}{D/\lambda}$ for fewer pedestrians is less than that for more pedestrians. This is because pedestrians acting like cause additional power loss. This is because pedestrians acting like cause additional power loss. The effect of pedestrians increases as A increasing. [22] says that pedestrians act as a lossy dielectric component of rectangular waveguide below 5-6 GHz, and act as highly lossy obstacles for radio propagation above 6-7 GHz.

3.6 Branch Tunnels

- {#49, #16}, {#51, #19}: For the two branched tunnels (#48 to #51), LOS signal disappears in the BBP region, causing a big power loss, so $100\frac{P_L}{D/\lambda}(BBP)$ for the branched tunnels is bigger than that for the straight tunnels.

Chapter 4

Other Observations

- In straight empty tunnels, $100\frac{P_L}{D/\lambda}(BBP)$ is bigger than $100\frac{P_L}{D/\lambda}(ABP)$. This can be explained as follows: ABP part of a straight tunnel is the far distance region to the transmitter compared with BBP part. In ABP part, LOS signal dominates the transmission, because the effect of multi-path components is weakened compared with BBP part, due to many times of reflection and the longer path difference between direct wave and reflected wave as receiver moving further away from transmitter, so less fluctuation leads a smaller $\frac{P_L}{D/\lambda}$ in ABP part of a tunnel than BBP part. This agrees with the conclusion in [20]
- {#1, #2, #3}: For VV, $100\frac{P_L}{D/\lambda}(BBP)$ decreases with decreasing R. #1 and #2's larger A would have produced a smaller $100\frac{P_L}{D/\lambda}(BBP)$, but for its large R. The relation is reversed for ABP part, because LOS signal dominates the transmission in ABP part and R is not as important as in the BBP part. #1 and #2's bigger A gives them a smaller $100\frac{P_L}{D/\lambda}(ABP)$ than #3, despite #3's smaller R.
- {#6, #13}: The effect of mismatch between polarization and cross-sectional shape decreases with increasing A. #6's horizontal polarization would have a smaller $100\frac{P_L}{D/\lambda}(BBP)$ than that for #13 in tunnels whose R is bigger than 1, but for the #13' larger A.
- {#1, #2, #9}: Agree with $100\frac{P_L}{D/\lambda}(BBP)$ and $100\frac{P_L}{D/\lambda}(ABP)$ decrease with C_{Tx} approaching 0.5. α increases as C_{Tx} approaching 0.5.
- {#10, #29}: In BBP part, #10's larger A overrides its smaller R and less favorable C_{Tx}, so its $100\frac{P_L}{D/\lambda}(BBP)$ is smaller than that for #29, but in ABP part, #29 has a smaller $100\frac{P_L}{D/\lambda}(ABP)$ than that for #10. As mentioned before, the effect of R is weakened in ABP part, so the reason why #29's $100\frac{P_L}{D/\lambda}(ABP)$

becomes smaller is its favorable C_{Tx}. Hence, the current author has a conclusion: in BBP part, since signal's power is about equally from the reflected signal and LOS signal, A is the dominant factor for signal's transmission, the effect of other factors can be attenuated by enlarging A; While in ABP part, since LOS signal dominates the transmission and the reflected signal does not affect as much as in BBP, C_{Tx} and C_{Rx} become the dominant factor. The signal would have the smallest $100\frac{P_L}{D/\lambda}(ABP)$ if C_{Tx} = 0.5 and C_{Rx} = 0.5. This because in the central place of a tunnel, LOS signal receives the least interference.

- Data sets from #77 to #82: Curved tunnel has bigger $\frac{P_L}{D/\lambda}$ than that for straight tunnel, due to curvature loss [20].
- {#62, #64}: Curvance can lead extra propagation loss thus larger $100\frac{P_L}{D/\lambda}(BBP)$ and $100\frac{P_L}{D/\lambda}(ABP)$. The ABP part of {#61, #63}: Curvance can lead extra propagation loss thus larger $100\frac{P_L}{D/\lambda}(ABP)$. #63 and #64's larger A and favorable C_{Tx} would cause smaller $\frac{P_L}{D/\lambda}$ for both BBP and ABP parts but for the curvance. \#63: The curvance, after which no LOS signal exists, will increase $100\frac{P_L}{D/\lambda}(ABP)$ a lot. The curvance occurs in the ABP part of tunnel and leads no LOS signal for this part, so $100\frac{P_L}{D/\lambda}(ABP)$ increases and it is even bigger than its counterpart for BBP. This can be explained as follows. In ABP part, the signal's power is mainly from LOS component, no LOS signal means a huge power loss thus lead a very larger $100\frac{P_L}{D/\lambda}(ABP)$.
- {#50, #19}, {#48, #17}: $100\frac{P_L}{D/\lambda}(ABP)$ for the branched tunnel is bigger than that for the straight tunnel. This can be explained as follows. As the receiver moved from the branch tunnel into the main one in a close distance from the transmitter, the distance for the break point to appear is shortened, so the ABP region for this branched tunnel is not as far as that for the straight tunnel and the reflected components are not attenuated as much as those in straight tunnels. This will cause a large fluctuation in the ABP region, although no LOS signal, and so a bigger $100\frac{P_L}{D/\lambda}(ABP)$ for this branched tunnel compared with the straight tunnel.
- {#40, #9}: $100\frac{P_L}{D/\lambda}(BBP)$ for arched cross-sectional shape is larger than that for rectangular cross-sectional shape. #40's larger A would have a smaller

$100\frac{P_L}{D/\lambda}(BBP)$ than that for #9, but for its arched cross-sectional shape. {#33, #41}, {#9, #41}, {#9, #42}, {#12, #42}, or {#12, #43} agree with this conclusion.

- {#40, #9}, {#41, #9}, {#42, #9}, or {#43, #9}: $100\frac{P_L}{D/\lambda}(ABP)$ for arched cross-sectional shape is larger than that for rectangular cross-sectional shape.
- {#43, #9}: The effect of polarization is decreased in the ABP part compared with BBP part. $100\frac{P_L}{D/\lambda}(BBP)$ of #43 is smaller that of #9 due to #43's horizontal polarization and the tunnel's R, which is larger than 1. But for $100\frac{P_L}{D/\lambda}(ABP)$, there is a reverse result. This is because in ABP, the reflected components are not as important as in BBP, so the decreasing of $100\frac{P_L}{D/\lambda}(ABP)$ due to favorable polarization is small.
- {#17, #38}, {#17, #60}, {#16, #39}: $100\frac{P_L}{D/\lambda}(BBP)$ for arched cross-sectional shape is larger than that for rectangular cross-sectional shape.
- {#17, #60}, {#17, #38}, {#19, #39}: $100\frac{P_L}{D/\lambda}(ABP)$ for arched cross-sectional shape is larger than that for rectangular cross-sectional shape.
- {#16, #39}: Polarization for ABP is not as important as for BBP: $100\frac{P_L}{D/\lambda}(BBP)$ of #16 is smaller than that for #39 due to its bigger R, but this is not true in the ABP part, where #39's $100\frac{P_L}{D/\lambda}(ABP)$ is smaller than that for #16 due to its larger A.
- {#14, #23}: $100\frac{P_L}{D/\lambda}(BBP)$ for brick tunnels is larger than that for coal mine tunnels. #23's smaller R and larger A would have a smaller $100\frac{P_L}{D/\lambda}(BBP)$, but for the tunnel wall's material.
- {#11, #29}, or {#19, #29}: $100\frac{P_L}{D/\lambda}(BBP)$ for potash tunnel is larger than that for coal mine tunnels. #29's larger R and A would have a smaller $100\frac{P_L}{D/\lambda}(BBP)$ but for its tunnel wall's material.
- {#14, #23}, $\{\#11,\#29\}$: $\frac{P_L}{D/\lambda}$ is inversely proportioned to the dielectric constant of tunnel walls. There are two physical constants for tunnel walls: conductivity(μ) and dielectric constant(ε). For potash tunnels, the common settings are μ = 6 and ε = 0.0001 s/m; for coal mine tunnels, μ = 10 and ε = 0.01 s/m. Because at frequencies above the VHF band, the surrounding material acts

as a pure dielectric [8], the ohmic loss related to μ is negligible and the refraction loss related to ε plays a dominant role in the attenuation. Only considering ε, potash tunnels with a smaller ε have a larger $\frac{P_L}{D/\lambda}$ than coal mine tunnels with a larger ε; brick tunnels with ε = 4.5 have a larger $\frac{P_L}{D/\lambda}$ than coal mine tunnels.

- {#61, #42}, or {#61, #43}: In BBP part of tunnel, $\frac{P_L}{D/\lambda}$ for railway tunnels is smaller than that for concrete tunnels: data sets {#61, #42}, or {#61, #43}. #61's smaller A would produce a larger $\frac{P_L}{D/\lambda}$ but for its tunnel material. The current author thinks that in a railway tunnel or subway tunnel, there are several things which do not exist in other tunnels, like rails on the floor and cables on the wall. These things go through the whole tunnels, acting like small wave guides and reflectors. So this can attenuate power loss thus produce a smaller $\frac{P_L}{D/\lambda}$. This agrees with [19] which avoids significant propagation loss by putting artificial reflectors on the walls.
- {#50, #49}, {#48, #17}: α for branched tunnel is larger than that for straight tunnels.

Chapter 5

Empirical Data

Empirical Data 1

Data Set	Reference	Tunnel Cross-section Shape	λ	R	W/λ	H/λ	Tunnel Longitudinal Shape	TX's Position	Tunnel Wall Materials	Obstacle or Empty	C_{Tx}	C_{Rx}	T_x^{π}	T_x^{π}	R_e	R_R	Tx-Rx Polarizations	Break Point's Longitudinal position (λ)	Break Point's Position by Formula	$10\log\frac{P_r}{P_t}(dB\ P)$	$10\log\frac{P_r}{P_t}(dB/\lambda)$	$10\log\frac{P_r}{P_t}(\Delta\ dB\ P)$	α	$10\log\frac{P_r}{P_t}(\Delta\ dB/\lambda)$
#1	[41] Fig. 3	Rectangular	270	1.88	22.50	12.00	Straight	*	Concrete	Empty	0.30	0.20	0.30	0.30	0.20	0.30	VV	120	506	23.87	0.86	27.6	*
#2	[24] Fig. 3	Rectangular	270	1.88	22.50	12.00	Straight	Inside	Concrete	Empty	0.25	0.20	0.25	0.30	0.20	0.30	VV	120	506	27.83	1.45	19.2	*
#3	[34] Fig. 4a	Rectangular	147	0.88	11.40	12.90	Straight	Inside	US, Concrete	Empty	0.27	*	0.27	0.66	*	*	VV	60	166	16.90	1.57	10.8	*	*
#4	[34] Fig. 4b	Rectangular	588	0.88	22.80	25.80	Straight	Inside	US, Concrete	Empty	0.49	*	0.51	0.51	*	*	VV	600	666	2.29	*	*	*	*
#5	[41] Fig. 6	Rectangular	623	0.88	23.47	26.36	Straight	*	Subway	Empty	0.50	*	0.50	0.50	*	*	VV	638	705	1.25	*	*	*	*
#6	[41] Fig. 7	Rectangular	2177	1.17	50.40	43.20	Straight	*	Concrete	Empty	0.50	0.40	0.50	0.50	0.60	0.50	HH	2400	1866	0.65	0.03	19.5	*	*
#7	[20] Fig. 4a	Rectangular	76	1.07	9.00	8.40	Straight	*	Concrete(COMB)	Empty	0.50	0.60	0.50	0.50	0.60	0.60	HH	120	81	13.93	10.83	1.3	*	*
#8	[12] Fig. 2a	Rectangular	338	1.30	24.00	14.80	Straight	*	Concrete	Empty	0.50	0.50	0.50	0.50	0.50	0.50	VV	480	576	*	*	*	*	0.97
#9	[12] Fig. 3a	Rectangular	405	1.69	25.50	15.90	Straight	*	Concrete	Empty	0.50	0.50	0.50	0.50	0.50	0.50	VV	1350	650	1.83	0.23	7.9	*	*
#10	[10] Fig. 3	Rectangular	230	2.27	22.86	10.06	Straight	Inside	Potash	Empty	0.14	0.45	0.50	0.86	0.50	0.45	HH	150	523	5.00	2.30	2.2	*	*
#11	[41] Fig. 2	Rectangular	126	1.14	12.00	10.30	Straight	*	Coal mine	Empty	0.15	0.15	0.15	0.44	0.15	0.44	HH	360	144	5.73	*	*	*	*
#12 $^{+}$	[39] Fig. 5	Rectangular	785	2.39	43.32	18.12	Straight	*	Concrete	Empty	0.16	0.16	0.16	0.16	0.50	0.16	VV	*	1876	1.26	*	*	*	*
#13 $^{+}$	[39] Fig. 6	Rectangular	6030	2.39	120.05	50.23	Straight	*	Concrete	Empty	0.16	0.16	0.16	0.16	0.50	0.16	VV	*	1442	0.26	*	*	*	*
#14	[1] Fig. 9	Rectangular	17	2.00	5.90	2.95	Straight	*	Coal mine	Empty	*	*	*	*	*	*	VV	138	35	24.36	16.70	1.5	*	*
#15	[1] Fig. 9	Rectangular	17	2.00	5.90	2.95	Straight	*	Coal mine	Empty	*	*	*	*	*	*	HV	138	35	20.60	15.76	1.3	*	*
#16	[1] Fig. 9	Rectangular	17	2.00	5.90	2.95	Straight	*	Coal mine	Empty	*	*	*	*	*	*	HH	138	35	15.11	13.59	1.1	*	*
#17	[1] Fig. 10	Rectangular	101	2.00	14.22	7.11	Straight	*	Coal mine	Empty	*	*	*	*	*	*	VV	333	202	6.48	2.88	2.3	*	*
#18	[1] Fig. 10	Rectangular	101	2.00	14.22	7.11	Straight	*	Coal mine	Empty	*	*	*	*	*	*	HV	333	202	8.19	2.97	2.8	*	*
#19	[1] Fig. 10	Rectangular	101	2.00	14.22	7.11	Straight	*	Coal mine	Empty	*	*	*	*	*	*	HH	333	202	4.41	2.85	2.5	*	*
#20	[20] Fig. 6	Rectangular	43	1.20	7.20	6.00	Straight	*	Brick(SMT)	Empty	0.10	0.50	0.10	0.70	0.50	0.50	VV	60	52	34.83	9.30	3.7	*	*
#21	[20] Fig. 6	Rectangular	43	1.20	7.20	6.00	Straight	*	Brick(SMT)	Empty	0.10	0.50	0.50	0.90	0.50	0.50	VV	60	52	19.57	8.70	2.2	*	*
#23	[20] Fig. 6	Rectangular	43	1.20	7.20	6.00	Straight	*	Brick(SMT)	Empty	0.50	0.50	0.50	0.50	0.50	0.50	VV	60	52	26.23	9.00	2.9	*	*
#22 $^{\diamond}$	[15] Fig. 3a	Rectangular	3538	5.29	186.67	23.83	Straight	Inside	Platform	Empty	0.27	*	0.27	0.48	*	*	VV	*	18678	0.79	*	*	*	*
#24 $^{\diamond}$	[30]	Rectangular	8	1.20	3.00	2.50	Straight	*	Bauxite	Empty	*	*	*	*	*	*	VV	*	*	*	*	*	*	6.400
#25	[30] Fig. 1b	Rectangular	68	1.20	9.00	7.50	Straight	*	Bauxite	Empty	*	*	*	*	*	*	VV	105	81	18.00	6.27	2.9	*	*
#26	[30] Fig. 2b	Rectangular	270	1.20	18.00	15.00	Straight	*	Bauxite	Empty	*	*	*	*	*	*	VV	340	324	6.77	1.57	4.3	*	*
#27	[35] Fig. 5	Rectangular	216	3.19	26.23	8.24	Straight	Inside	Potash	Empty	0.50	0.50	0.50	0.50	0.50	0.50	VV	366	688	6.49	2.23	2.9	*	*
#28	[35] Fig. 4	Rectangular	216	3.19	26.23	8.24	Straight	Inside	Potash	Empty	0.50	0.50	0.50	0.50	0.50	0.50	HH	366	688	6.39	1.44	4.4	*	*
#29 $^{+}$	[23] Fig. 8	Rectangular	1899	1.66	56.00	33.75	Straight	Inside	Train tunnel	Empty	0.21	0.30	0.50	0.79	0.30	0.53	*	*	3136	0.99	*	*	*	*
#30 $^{+}$	[44] Fig. 1	Rectangular	270	1.20	18.00	15.00	Straight	Entrance	Subway	Empty	*	*	*	*	*	*	VV	*	324	*	*	*	*	1.70
#32 $^{\diamond}$	[37] Fig. 3	Rectangular	236	0.60	11.89	19.81	Straight	Inside	Concrete(hallway)	Empty	0.33	0.33	0.67	0.66	0.67	0.66	VV	*	393	3.38	*	*	*	*
#33 $^{\diamond}$	[37] Fig. 3	Rectangular	236	0.60	11.89	19.81	Straight	Inside	Concrete(hallway)	Empty	0.33	0.33	0.67	0.66	0.67	0.66	HH	*	393	3.89	*	*	*	*
#34 $^{\diamond}$	[37] Fig. 3	Rectangular	236	0.60	11.89	19.81	Straight	Inside	Concrete(hallway)	Empty	0.33	0.33	0.67	0.66	0.67	0.66	VH	*	393	4.18	*	*	*	*
#35 $^{\diamond}$	[37] Fig. 3	Rectangular	236	0.60	11.89	19.81	Straight	Inside	Concrete(hallway)	Empty	0.33	0.33	0.67	0.66	0.67	0.66	HV	*	393	4.22	*	*	*	*
#37 $^{\diamond}$	[5] Fig. 4	Circle	141	1.00	6.70	6.70	Straight	Inside	Concrete	Empty	*	*	*	*	*	*	*	*	*	*	*	*	*	8.700
#78 $^{\diamond}$	[5] Fig. 4	Circle	317	1.00	10.05	10.05	Straight	Inside	Concrete	Empty	*	*	*	*	*	*	*	*	*	*	*	*	*	4.990
#79 $^{\diamond}$	[5] Fig. 4	Circle	1566	1.00	22.33	22.33	Straight	Inside	Concrete	Empty	*	*	*	*	*	*	*	*	*	*	*	*	*	0.250
#80 $^{\diamond}$	[5] Fig. 4	Circle	14095	1.00	67.00	67.00	Straight	Inside	Concrete	Empty	*	*	*	*	*	*	*	*	*	*	*	*	*	0.084
#81 $^{\diamond}$	[5] Fig. 4	Circle	47336	1.00	122.83	122.83	Straight	Inside	Concrete	Empty	*	*	*	*	*	*	*	*	*	*	*	*	*	0.009
#82 $^{\diamond}$	[5] Fig. 4	Circle	100234	1.00	178.67	178.67	Straight	Inside	Concrete	Empty	*	*	*	*	*	*	*	*	*	*	*	*	*	0.005

Empirical Data 2

Data Set	Reference	Tunnel Cross-section Shape	A	R	W/λ	H/λ	Tunnel Longitude Shape	Tx's Position	Tunnel Wall Materials	Obstacle or Empty	σ_{Tx}	σ_{Rx}	T_w	T_λ	R_w	R_λ	Tx-Rx Polarization	Break Point's Longitudinal position (λ)	Break Point's Position by Formula	$10\frac{P_L}{\lambda}(BBP)$ (dB/λ)	$10\frac{P_L}{\lambda}(ABP)$ (dB/λ)	σ	$10\frac{P_L}{\lambda}$ (dB/λ)
#83[*]	[5] Fig. 3	Circle	729	1.00	15.28	15.28	Curved	Inside	Concrete,ated	Empty	*	*	*	*	*	*	*	*	*	*	*	*	2.500
#84[*]	[5] Fig. 3	Circle	1641	1.00	22.86	22.86	Curved	Inside	Concrete,ated	Empty	*	*	*	*	*	*	*	*	*	*	*	*	1.410
#85[*]	[5] Fig. 3	Circle	8103	1.00	50.80	50.80	Curved	Inside	Concrete,ated	Empty	*	*	*	*	*	*	*	*	*	*	*	*	1.000
#86[*]	[5] Fig. 3	Circle	72929	1.00	152.40	152.40	Curved	Inside	Concrete,ated	Empty	*	*	*	*	*	*	*	*	*	*	*	*	0.200
#87[*]	[5] Fig. 3	Circle	245122	1.00	279.40	279.40	Curved	Inside	Concrete,ated	Empty	*	*	*	*	*	*	*	*	*	*	*	*	0.100
#88[*]	[5] Fig. 3	Circle	518605	1.00	406.40	406.40	Curved	Inside	Concrete,ated	Empty	*	*	*	*	*	*	*	*	*	*	*	*	0.040
#38	[24] Fig. 4b	Arched	120	1.40	12.60	9.00	Straight	*	Coal mine	Empty	0.24	*	0.24	0.50	*	*	VV	135	159	22.67	8.27	2.7	*
#39	[24] Fig. 4a	Arched	120	1.40	12.60	9.00	Straight	*	Coal mine	Empty	0.24	*	0.24	0.50	*	*	HH	120	159	20.68	5.57	3.7	*
#36[+]	[2] Fig. 6a	Arched	1	1.25	1.28	1.03	Straight	Outside	Concrete	Empty	0.33	0.33	0.33	0.47	0.33	0.47	HH	*	*	*	*	*	226.50
#37[+]	[2] Fig. 6b	Arched	3	1.25	1.92	1.54	Straight	Outside	Concrete	Empty	0.33	0.33	0.33	0.47	0.33	0.47	HH	*	*	*		* *	108.50
#52[+]	[2] Fig. 6c	Arched	16	1.25	4.80	3.85	Straight	Outside	Concrete	Empty	0.33	0.33	0.33	0.47	0.33	0.47	HH	*	*	*	*	*	22.60
#53[+]	[2] Fig. 6d	Arched	157	1.25	15.04	12.08	Straight	Outside	Concrete	Empty	0.33	0.33	0.33	0.47	0.33	0.47	HH	*	*	*	*	*	0.63
#54[+]	[2] Fig. 6e	Arched	576	1.25	28.80	23.10	Straight	Outside	Concrete	Empty	0.33	0.33	0.33	0.47	0.33	0.47	HH	*	*	*	*	*	0.07
#55[+]	[2] Fig. 7a	Arched	1	1.25	1.28	1.03	Straight	Outside	Concrete	Empty	0.33	0.33	0.33	0.47	0.33	0.47	VV	*	*	*	*	*	262.50
#56[+]	[2] Fig. 7b	Arched	3	1.25	1.92	1.54	Straight	Outside	Concrete	Empty	0.33	0.33	0.33	0.47	0.33	0.47	VV	*	*	*	*	*	155.00
#57[+]	[2] Fig. 7c	Arched	16	1.25	4.80	3.85	Straight	Outside	Concrete	Empty	0.33	0.33	0.33	0.47	0.33	0.47	VV	*	*	*	*	*	37.20
#58[+]	[2] Fig. 7d	Arched	157	1.25	15.04	12.08	Straight	Outside	Concrete	Empty	0.33	0.33	0.33	0.47	0.33	0.47	VV	*	*	*	*	*	0.63
#59[+]	[2] Fig. 7e	Arched	576	1.25	28.80	23.10	Straight	Outside	Concrete	Empty	0.33	0.33	0.33	0.47	0.33	0.47	VV	*	*	*	*	*	0.07
#60	[31] Fig. 3	Arched	120	1.40	12.60	9.00	Straight	Inside	Coal mine	Empty	0.24	*	0.24	0.50	*	*	VV	135	159	13.70	6.77	2.0	*
#41	[40] Fig. 5	Arched	505	1.61	31.45	19.50	Straight	Inside	Concrete	Empty	*	*	*	*	*	*	HH	314	989	4.29	0.51	8.4	*
#40	[40] Fig. 6	Arched	505	1.61	31.45	19.50	Straight	Inside	Concrete	Empty	*	*	*	*	*	*	VV	314	989	7.31	0.64	11.5	*
#43	[40] Fig. 7	Arched	1880	1.61	60.65	37.75	Straight	Inside	Concrete	Empty	*	*	*	*	*	*	HH	910	3679	1.76	0.26	6.7	*
#42	[40] Fig. 8	Arched	1880	1.61	60.65	37.75	Straight	Inside	Concrete	Empty	*	*	*	*	*	*	VV	758	3679	1.98	0.38	5.2	*
#61	[42] Fig. 3a	Half circle	603	2.00	39.20	19.60	Straight	Inside	Railway	Empty	0.17	0.17	0.50	0.83	0.50	0.83	*	16333	1337	0.24	0.16	1.5	*
#62	[42] Fig. 3b	Half circle	10048	2.00	160.00	80.00	Straight	Inside	Railway	Empty	0.17	0.17	0.50	0.83	0.50	0.83	*	66667	25000	0.04	0.03	1.3	*
#63	[42] Fig. 5a	Half circle	1354	2.00	58.80	29.40	Curved	Inside	Railway	Empty	0.33	0.33	0.33	0.56	0.33	0.56	*	8167	3457	0.11	0.17	0.6	*
#64	[42] Fig. 5b	Half circle	22556	2.00	240.00	120.00	Curved	Inside	Railway	Empty	0.33	0.33	0.33	0.56	0.33	0.56	*	50000	57600	0.05	0.04	1.1	*
#50	[24] Fig. 5a	Rectangular	113	1.40	12.60	9.00	Branched	Inside	Coal mine	Empty	*	*	*	*	*	*	HH	60	159	101.40	6.27	16.2	*
#48	[24] Fig. 5b	Rectangular	113	1.40	12.60	9.00	Branched	Inside	Coal mine	Empty	*	*	*	*	*	*	VV	56	159	104.10	7.27	14.3	*
#49[+]	[1] Fig. 6	Rectangular	17	2.00	5.90	2.95	Branched	*	Coal mine	Empty	*	*	*	*	*	*	HH	*	54.29	*	*	*	*
#51[+]	[1] Fig. 7	Rectangular	101	2.00	14.22	7.11	Branched	*	Coal mine	Empty	*	*	*	*	*	*	HH	*	21.51	*	*	*	*
#65	[28] Fig. 6a	Rectangular	113	1.40	12.60	9.00	Straight	Entrance	Concrete	trucks	*	*	*	*	*	*	VV	120	159	33.80	0.33	101.4	*
#66[α]	[22] Fig. 2a	Rectangular	65	2.13	11.73	5.50	Straight	Inside	Subway street	More pedestrians	0.50	0.33	0.50	0.50	0.50	0.33	VV	*	*	*	*	*	20.18
#95[α]	[22] Fig. 2a	Rectangular	65	2.13	11.73	5.50	Straight	Inside	Subway street	Less pedestrians	0.50	0.33	0.50	0.50	0.50	0.33	VV	*	*	*	*	*	17.65
#67[α]	[22] Fig. 2b	Rectangular	65	2.13	11.73	5.50	Straight	Inside	Subway street	More pedestrians	0.50	0.33	0.50	0.50	0.50	0.33	HH	*	*	*	*	8	12.00
#96[α]	[22] Fig. 2b	Rectangular	65	2.13	11.73	5.50	Straight	Inside	Subway street	Less pedestrians	0.50	0.33	0.50	0.50	0.50	0.33	HH	*	*	*	*	*	11.67
#68[α]	[22] Fig. 2c	Rectangular	213	2.13	21.33	10.00	Straight	Inside	Subway street	Pedestrians	0.50	0.33	0.50	0.50	0.50	0.33	VV	*	*	*	*	*	5.34
#69[α]	[22] Fig. 2d	Rectangular	213	2.13	21.33	10.00	Straight	Inside	Subway street	Pedestrians	0.50	0.33	0.50	0.50	0.50	0.33	HH	*	*	*	*	*	4.35
#70[α]	[22] Fig. 2e	Rectangular	9013	2.13	138.67	65.00	Straight	Inside	Subway street	Pedestrians	0.50	0.33	0.50	0.50	0.50	0.33	VV	*	*	*	*	*	0.51
#71[α]	[22] Fig. 2f	Rectangular	9013	2.13	138.67	65.00	Straight	Inside	Subway street	Pedestrians	0.50	0.33	0.50	0.50	0.50	0.33	HH	*	*	*	*	*	0.60
#72[α]	[22] Fig. 2g	Rectangular	21333	2.13	213.33	100.00	Straight	Inside	Subway street	More pedestrians	0.50	0.33	0.50	0.50	0.50	0.33	VV	*	*	*	*	59 *	0.56
#97[α]	[22] Fig. 2g	Rectangular	21333	2.13	213.33	100.00	Straight	Inside	Subway street	Less pedestrians	0.50	0.33	0.50	0.50	0.50	0.33	VV	*	*	*	*	*	0.26
#73[α]	[22] Fig. 2h	Rectangular	21333	2.13	213.33	100.00	Straight	Inside	Subway street	More pedestrians	0.50	0.33	0.50	0.50	0.50	0.33	HH	*	*	*	*	*	0.50
#98[α]	[22] Fig. 2h	Rectangular	21333	2.13	213.33	100.00	Straight	Inside	Subway street	Less pedestrians	0.50	0.33	0.50	0.50	0.50	0.33	HH	*	*	*	*	*	0.26

Empirical Data 3

Data Set	Reference	Tunnel Cross-section Shape	A	R	W/λ	H/λ	Tunnel Longitudinal Shape	Tx's Position	Tunnel Wall Materials	Obstacle or Empty	C_{Tx}	C_{Rx}	T_H	T_V	R_H	R_V	Tx-Rx Polarizations	Break Point's Longitudinal position (λ)	Break Point's Position by Formula	$1.0\frac{F_1}{\lambda}$ (HBP) (dB/λ)	$1.0\frac{F_1}{\lambda}$ (ABP) (dB/λ)	σ	$1.0\frac{F_1}{\lambda}$ (dB/λ)
#74	[31] Fig. 3	Arched	120	1.40	12.00	9.00	Straight	Inside	Coal mine	Trolleys	0.24	*	0.24	0.50	*	*	VV	135	159	20.60	7.27	2.8	*
#75	[31] Fig. 4	Arched	120	1.40	12.60	9.00	Straight	Inside	Coal mine	Belt	0.28	*	0.24	0.50	*	*	VV	135	159	30.67	2.17	14.2	*
#76$^+$	[40] Fig. 2	Rectangular	270	1.20	18.00	15.00	Straight	Entrance	Subway	Train	*	*	*	*	*	*	VV	*	324	*	*	*	2.55
#84	[34] Fig. 5	Arched	208	1.26	17.40	13.80	Curved	Inside	Subway(U8)	Empty	0.33	*	0.67	0.54	*	*	VV	300	303	4.37	1.00	4.4	*
#85	[34] Fig. 6	Arched	832	1.26	34.80	27.60	Curved	Inside	Subway(U8)	Empty	0.33	*	0.34	0.53	*	*	VV	900	1211	2.07	0.72	2.9	*
#89$^+$	[20] Fig. 4b	Rectangular	832	1.32	20.58	15.60	Curved	*	Concrete(NS175)	Empty	0.50	0.00	0.50	0.50	0.50	0.00	HH	*	*	*	*	*	26.08
#87$^+$	[27] Fig. 4a	Arched	20000	1.13	150.00	133.33	Curved	*	Concrete	Empty	0.50	*	0.50	0.50	*	*	VV	*	22500	*	*	*	0.04
#88$^+$	[27] Fig. 4b	Arched	800	1.13	30.00	26.67	Curved	*	Concrete	Empty	0.50	*	0.50	0.50	*	*	VV	*	900	*	*	*	0.27
#90$^+$	[44] Fig. 1	Rectangular	495	2.00	33.00	15.00	Curved	Entrance	Subway	Empty	*	*	*	*	*	*	VV	*	1089	*	*	*	7.65
#91$^+$	[42] Fig. 4a	Half circle	605	1.13	39.20	19.60	Curved	Inside	Railway	Empty	0.17	0.17	0.50	0.85	0.50	0.85	*	*	1537	*	*	*	0.18
#92$^+$	[42] Fig. 4b	Half circle	10044	2.00	160.00	80.00	Curved	Inside	Railway	Empty	0.17	0.17	0.50	0.85	0.50	0.85	*	*	25600	*	*	*	0.04
#93	[42] Fig. 5a	Half circle	1354	2.00	58.80	29.40	Curved	Inside	Railway	Empty	0.33	0.33	0.33	0.56	0.33	0.56	*	8167	3457	0.11	0.17	0.6	*
#94	[42] Fig. 5b	Half circle	22556	2.00	240.00	120.00	Curved	Inside	Railway	Empty	0.33	0.33	0.33	0.56	0.33	0.56	*	96667	57600	0.03	0.04	0.8	*
#99$^+$	[28] Fig. 2	Arched	5488	2.29	112.00	49.00	Straight	Inside	Concrete	Low traffic	0.13	0.29	0.13	0.29	0.38	0.29	*	*	12544	*	*	*	0.17
#100$^+$	[28] Fig. 2	Arched	5488	2.29	112.00	49.00	Straight	Inside	Concrete	High traffic	0.13	0.29	0.13	0.29	0.38	0.29	*	*	12544	*	*	*	0.54
#101$^+$	[25] Fig. 1	Rectangular	4622	1.63	86.67	53.33	Straight	Inside	Concrete	Empty	0.15	0.15	0.15	0.25	0.15	0.25	VV	*	12544	*	*	*	0.65
#102	[46] Fig. 1	Circle	140	1.00	6.67	6.67	Straight	*	$\epsilon = 12, \mu = .02$	Empty	0.05	0.05	0.30	0.05	0.30	0.05	*	1667	44	1.39	0.24	6.6	*
#103	[32] Fig. 5	Rectangular	60420	1.90	191.40	100.53	Curved	Outside	Concrete	Empty	*	*	*	*	*	*	*	967	36634	1.02	0.28	3.6	*
#104	[32] Fig. 10	Rectangular	60420	1.90	191.40	100.53	Curved	Inside	Concrete	Empty	*	*	*	*	*	*	*	967	36634	5.10	2.59	1.2	*
#105$^+$	[45] Fig. 2	Rectangular	*	*	*	*	Curved	Inside	Concrete	Empty	*	*	*	*	*	*	*	*	*	*	*	*	2.50
#106$^+$	[45] Fig. 2	Rectangular	*	*	*	*	Curved	Inside	Concrete	Train	*	*	*	*	*	*	*	*	*	*	*	*	2.70

Appendix A

Details of Tunnels

- The TCMH tunnel complex consists of three main tunnels interconnected through several short branched tunnels. The tunnel complex was horizontally drilled in the western mountain. It has a slightly arched-shaped cross section and was reinforced with concrete. The central main tunnel is approximately 10 km long, 3.0 m high, and 4.2 m wide, and the branched one is 140 m long, 3.0 m high, and 2.8 m wide.
- The SIMT tunnel is a small part of the underground labyrinth built in 1970's. The substratum of the tunnel is composed of loess and is reinforced with bricks. This rectangular tunnel of a 200-m length, 2-m height, and 2.4-m width can be roughly divided into three sections with the entry one of 100 m being the longest.
- The U8 tunnel is a curved arched, single-lane tunnel. Its cross-section is constituted by a circular shape of radius $r_{cs} \approx 2.9$ m with an elevated floor 1.2 m above the lowest point of the circle. A schematic plot of the tunnel's course is shown in Fig. A-1. It consists of nine different sections. The total length of the tunnel is about 1079 m. At distances further than 420 m from the transmitter, the receiver and the transmitter no longer have a direct line-of-sight.

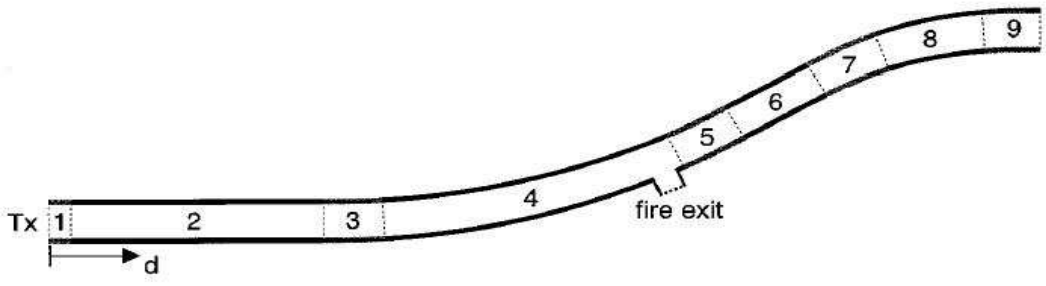

Figure A-1:U8 tunnel

- The U5 tunnel is a short, straight, rectangular, wide-profile single-lane tunnel section, with 3.8 m in width, 4.3 m in height, 110 m in length. The main material is reinforced concrete.
- An NS 173 tunnel constructed of concrete is a subway with a rectangular cross-section. The tunnel is 3.43 m wide, 2.6 m high, and 258.7 m long. It can be roughly divided into three sections. The middle section being 107.7 m long is straight while the two outer sections are slightly curved with the length of 51 and 100 m.
- The curved tunnel for #83 - #88: three bends that cover a nearly 120-degree angle in horizontal plane, and four bends in the vertical plane. These vertical bends encompass an elevation drop of nearly 200 feet.
- The curved tunnel in data sets #46 and #47 : 4.5 m wide, 4 m high, the radii of curvature are large, greater than 1 km, and the tunnel consists in a succession of right, straight, and left curves.
- The branched tunnel in data sets #48 and #50 : 4.2 m wide, 3 m high, the tunnel model is shown in Fig. A-2. The transmitter positioned in the middle of the branch tunnel was 10 m away from the junction formed by the branch and the main tunnel. The receiver was being moved from the branch tunnel into the main tunnel.

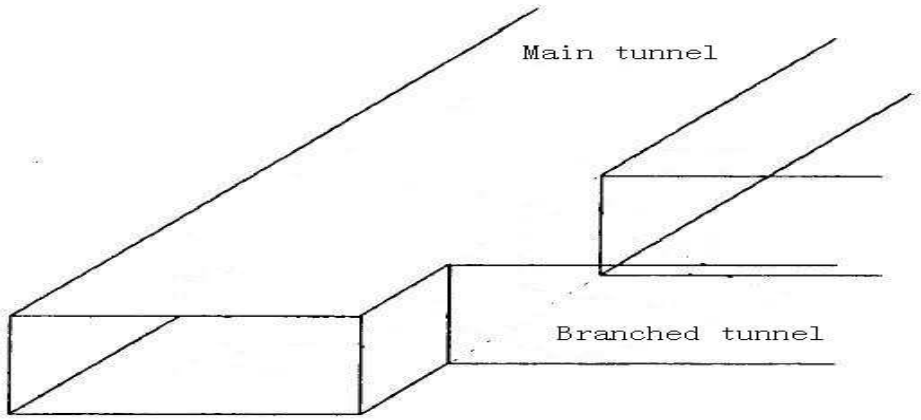

Figure A-2: Branched tunnel A

- The branched tunnel in data sets #49 and #51: 4.3 m wide, 2.1 m high, the tunnel model is shown in Fig. A-3. The transmitter was located in the main tunnel, and the receiver was being moved from the main tunnel to the cross tunnel.

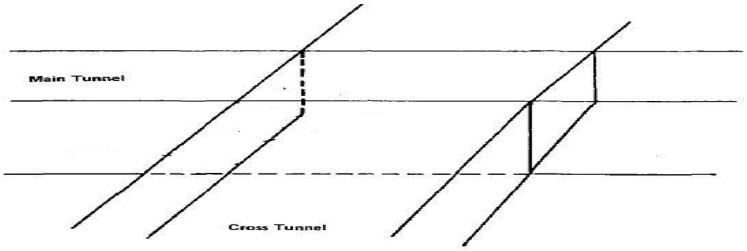

Figure A-3: Branched tunnel B

- The obstructed tunnel for data set #65: a truck is stopped 64 m away from the entrance.
- The obstructed tunnel for data set #74: 20 cascaded trolleys (1.5 m high, 1 m wide, 3 m long) stationed at 60 to 102 m.
- The obstructed tunnel for data set #75: a 2.0 m wide belt is permanently installed, 1.0 m above the floor.
- The curved tunnel for #90: a strong bend on length of 200 m.
- The tunnel in [42] is showed in Fig. A-4

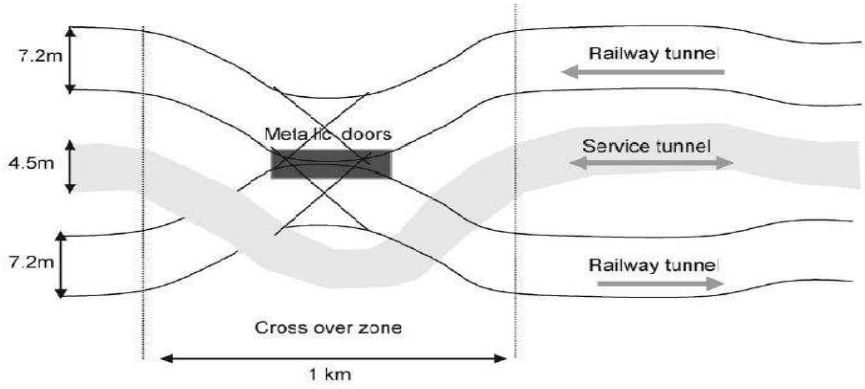

Figure A-4: Tunnel in [42]

- The road tunnel in [32] is showed in Fig. A-5

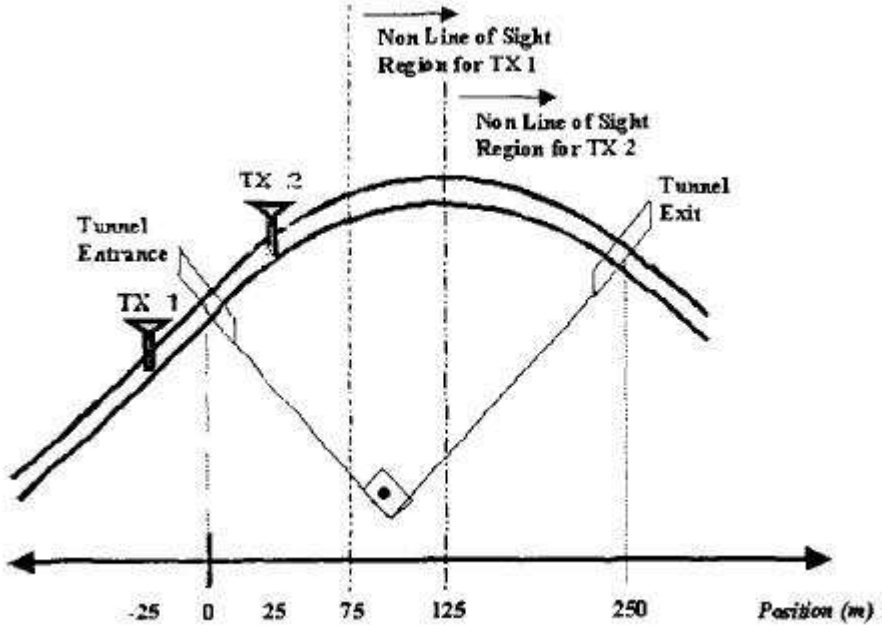

Figure A-5: Tunnel in [32]

- The subway tunnel in [45] is showed in Fig. A-6

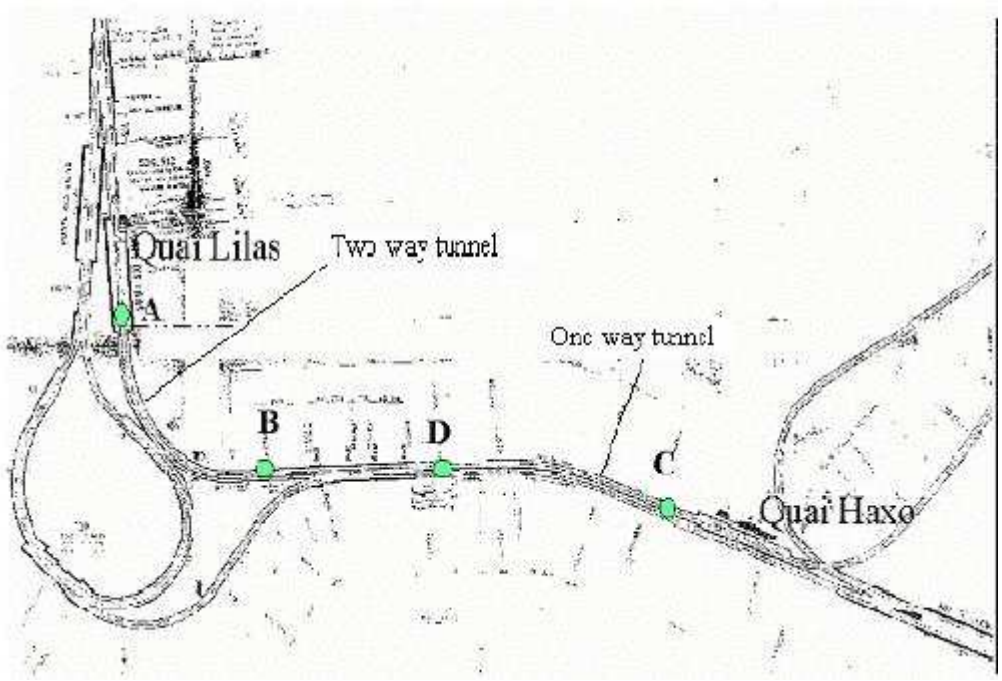

Figure A-6: Tunnel in [45]

Bibliography

[1] A. G. Emslie, R. L. Lagace, & P. F. Strong, ``Theory of the Propagation of UHF Radio Waves in Coal Mine Tunnels," *IEEE Transactions on Antenna & Propagation*, vol. 23, no. 2, pp. 192-205, March 1975.

[2] J. Chiba, T. Inaba, Y. Kuwamoto, O. Banno & R. Sato, ``Radio Communication In Tunnels," *IEEE Transactions on Microwave Theory and Techniques*, vol. 26, No. 6, pp. 439-443, June 1978.

[3] L. Deryck, ``Natural Propagation of Electromagnetic Waves in Tunnels," *IEEE Transactions on Vehicular Technology*, vol. 27, no. 3, pp. 145-150, August 1978.

[4] B. Jacard & O. Maldonado, ``Microwave Modeling of Rectangular Tunnels," *IEEE Transactions on Microwave Theory & Techniques*, vol. 32, no. 6, pp. 576-581, June 1984.

[5] J. De Haan & M. L. Jacobs, ``Tunnel Communication Test Results," *U.S. Bureau of Reclamation*, Project Notes 8450-98-06, January 1988.

[6] Y. Ohtaki, Y. Yamaguchi & T. Abe, "Experimental Study of Propagation Characteristics on Roads on a Snowy Mountain," *IEEE Transactions on Electromagnetic Compatibility*, vol. 30, no. 2, pp. 137-144, May 1988.

[7] Y. Yamaguchi, T. Abe & T. Sekiguchi, ``Radio Wave Propagation Loss in the VHF to Microwave Region Due to Vehicles in Tunnels," *IEEE Transaction on Electromagnetic Compatibility*, vol. 31, No. 1, pp. 87-91, February 1989.

[8] Y. Yamaguchi, T. Honda, M. Sengoku, S. Motooka & T. Abe, ``On the Reduction of Wave Propagation Loss in Tunnels," *IEEE Transactions on Electromagnetic Compatibility*, vol. 34, no. 2, pp. 78-85, May 1992.

[9] S. Chow, ``Propagation of Radio Waves in Potash Mine Tunnels and Its Implication on Radio Systems Performance," *Singapore International*

Conference on Computational Science / International Symposium on Information Theory and its Applications, pp. 890-894, 1992.

[10] J.-P. Saindon, ``Propagation of Radio Waves in Underground Tunnels and Underground Radio Systems," *IEEE International Conference on Antennas & Propagation*, vol. 1, pp. 155-158, 1993.

[11] H. H. Xia, H. L. Bertoni, L. R. Maciel, A. L. Stewart, & R. Rowe, "Radio Propagtion Characteristics for Line-of-Sight Microcellular and personal communications," *IEEE Trans. Antennas Propagate*, vol. 41, pp. 1439-1447, Oct. 1993.

[12] P. Mariage, M. Lienard & P. Degauque, ``Theoretical and Experimental Approach of the Propagation of High Frequency Waves in Road Tunnels," *IEEE Transactions on Antennas & Propagation*, vol. 42, no. 1, pp. 75-81, January 1994.

[13] T. Klemenschits, & E. Bonek, "Radio Coverage of Road Tunnels at 900 and 1800 MHz by Discrete Antennas," *The 5th Annual IEEE International Symposium on Personal, Indoor and Mobile Radio Communications*, pp. 411-415, September, 1994.

[14] Y. Hwary, & Y. P. Zhang, ``Variability of UHF Mobile Radio Signals in Tunnels," *International Symposium on Personal, Indoor, Mobile, Radio, Communications*, vol. 1, pp. 287-290, September 1994.

[15] S. Shinozaki, M. Wada, A. Teranishi, H. Furukawa & Y. Akaiwa, ``Radio Propagation Characteristics in Subway Platform and Tunnel in 2.5GHz Band," *International Symposium on Personal, Indoor, Mobile, & Radio Communications*, vol. 3, pp. 1175-1179, 1995.

[16] S.-H. Chen, & S.-K. Jeng, ``An SBR/Image Approach for Indoor Radio Propagation in a Corridor," *The Institute of Electronics, Information and Communication Engineers*, vol. E78-C, no. 8, pp. 1058-1062, August 1995.

[17] G. M. Whitman, K. S. Kim & E. Niver, ``A Theoretical Model for Radio Signal Attenuation Inside Buildings," *IEEE Transactions on Vehicular Technology*, vol. 44, no. 3, pp. 621-629, August 1995.

[18] S.-H. Chen, & S.-K. Jeng, ``SBR Image Approach for Radio Wave Propagation

in Tunnels with and Without Traffic," *IEEE Transactions on Vehicular Technology*, vol. 45, no. 3, pp. 570-578, August 1996.

[19] A. Kajiwara, ``Millimeter-Wave Indoor Radio Channel with Artificial Reflector," *IEEE Transactions on Vehicular Technology*, vol. 46, no. 2, pp. 486-493, May 1997.

[20] Y. P. Zhang & Y. Hwang, ``Characteristics of UHF Radio Propagation Channels in Tunnel Environments for Microcellular and Personal Communications," *IEEE Transactions on Vehicular Technology*, vol. 47, no. 1, pp. 283-296, February 1998.

[21] P. Aikio, R. Gruber & P. Vainikainen, ``Wideband Radio Channel Measurements for Train Tunnels," *IEEE Vehicular Technology Conference*, vol. 1, pp. 460-464, Spring 1998.

[22] Y. Yamaguchi, T. Abe & T. Sekiguchi, ``Radio Propagation Characteristics in Underground Streets Crowded with Pedestrians," *IEEE Transactions on Electromagnetic Compatibility*, vol. 30, no. 2, pp. 130-136, May 1998.

[23] R. P. Torres, L. Valle & M. Domingo, ``Analysis of Tunnels using CINDOOR Code,"

[24] Y. P. Zhang, Y. Hwang & R. G. Kouyoumjian, ``Ray-Optical Prediction of Radio-Wave Propagation Characteristics in Tunnel Environments-Part 2: Analysis and Measurements," *IEEE Transactions on Antenna & Propagation*, vol. 46, no. 9, pp. 1337-1345, September 1998.

[25] M. Lienard & P. Degauque, "Propagation in Wide Tunnels at 2 GHz: A Statistical Analysis," *IEEE Transactions on Vehicular Technology*, vol. 47, NO. 4, pp. 1322-1328, November, 1998.

[26] R. P. Torres, L. Valle, M. Domingo, S. Loredo & M. C. Diez, ``CINDOOR: An Engineering Tool for Planning and Design of Wireless Systems in Enclosed Spaces," *IEEE Antennas & Propagation Magazine*, vol. 41, no. 4, pp. 11-22, August 1999.

[27] M. Lienard, S. Betrencourt & P. Degauque, ``Theoretical and Experimental Approach of the Propagation at 2.5GHz and 10GHz in Straight and Curved

Tunnels," *IEEE Vehicular Technology Conference*, vol. 4, pp. 2268-2271, Fall 1999.

[28] S. Betrencourt, M. Lienard, & P. Degauque, "Mobile Communication in Road Tunnels: Influence of the Traffic Conditions on the Channel Characteristics," *10th Mediterranean Electrotechnical Conference*, vol. I, pp. 432-435, 2000.

[29] Y. P. Zhang, Z. R. Jiang, T. S. Ng & J. H. Sheng, ``Measurements of the Propagation of UHF Radio Waves on an Underground Railway Train," *IEEE Transactions on Vehicular Technology*, vol. 49, no. 4, pp.1342-1347, July 2000.

[30] M. Lienard & P. Degauque, ``"Natural Wave Propagation in Mine Environments," *IEEE Transactions on Antenna and Propagation*, vol. 48, no. 9, pp. 1326-1339, September 2000.

[31] ``Radio Propagation at 900 MHz in Underground Coal Mines," *IEEE Transactions on Antennas and Propagation*, vol. 49, no. 5, pp. 757-762, May 2001.

[32] A. V. B. da Silva & M. Nakagawa, "Radio Wave Propagation Measurements in Tunnel Entrance Environment for Intelligen Transportation Systems Applications," *IEEE Intelligent Transprotation Systems Conference Proceedings*, pp. 883-888, August, 2001.

[33] P. Kyritsi & D. C. Cox, ``Propagation Characteristics of Horizontally and Vertically Polarized Electric Fields in An Indoor Environment: Simple Model and Results," *IEEE Vehicular Technology Conference*, vol. 3, pp. 1422-1426, Fall 2001.

[34] D. Didascalou, J. Maurer & W. Wiesbeck, ``Subway Tunnel Guided Electromagnetic Wave Propagation at Mobile Communications Frequencies," *IEEE Transactions on Antennas & Propagation*, vol. 49, no. 11, pp. 1590-1596, November 2001.

[35] B. L. F. Daku, W. Hawkins & A. F. Prugger, ``Channel Measurements in Mine Tunnel," *IEEE Vehicular Technology Conference*, vol. 1, pp. 380-383, Spring 2002.

[36] W. Hawkins, B. L. F. Daku & A. F. Prugger, ``A Path Loss Measurement System

for Mines," *IEEE Canadian Conference on Electrical & Computer Engineering*, vol. 1, pp. 474-478, 2002.

[37] P. Kyritsi, D. C. Cox, R. A. Valenzuela & P. W. Wolniansky, ``Effect of Antenna Polarization on the Capacity of A Multiple Element System in An Indoor Environment," *IEEE Journal on Selected Areas in Communications*, vol. 20, no. 6, pp. 1127-1239, August 2002.

[38] M. Ndoh, G. Y. Delisle & R. Le, ``An Approach to Propagation Prediction in A Complex Mine Environment," *17th International Conference on Applied Electromagnetic and Communications*, pp. 237-240, 2003.

[39] Y. Kim, M. Jung & B. Lee, ``Analysis of Radio Wave Propagation Characteristics in Rectangular Road Tunnel at 800 MHz and 2.4 GHz," *IEEE Antennas and Propagation Society International Symposium*, vol. 3, pp. 1016-1019, 2003.

[40] T.-S. Wang & C.-F. Yang, ``Simulations and Measurements of Wave Propagations in Curved Road Tunnels for Signals from GSM Base Stations," *IEEE Antennas-Propagation Society International Symposium*, vol. 3, pp. 1012-1015, 2003.

[41] Y. P. Zhang, ``Novel Model for Propagation Loss Prediction in Tunnels," *IEEE Transactions on Vehicular Technology*, vol. 52, no. 5, pp. 1308-1314, September 2003.

[42] M. Lienard, P. Degauque & P. Laly, ``Long-Range Radar Sensor for Application in Railway Tunnels," *IEEE Transactions on Vehicular Technology*, vol. 53, no. 3, pp. 705-715, May 2004.

[43] H. Kwon, Y. Kim & B. Lee, ``Characteristics of Radio Propagation Channels in Tunnel Environments: A Statistical Analysis," *IEEE Antennas & Propagation Society International Symposium*, vol. 3, pp. 2995-2998, June 2004.

[44] M. Lienard & P. Degauque, ``Dual Antenna Array Systems in Tunnels: Propagation Channel Properties," *IEEE Antennas and Propagation Society International Symposium*, vol. 3, pp. 2971-2974, 2004.

[45] M. Lienard, P. Degauque & P. Laly, "Communication and Distance

Measurement in Subway Tunnels using Natural Propagation," *The Fifth IEEE International Caracas Conference on Devices, Circuits and Systems*, pp. 240-243, November 2004.

[46] D. G. Dudley, & H. Y. Pao, "System Identification for Wireless Propagation Channels in Tunnels," *IEEE Transactions on Antennas and Propagation*, vol. 53, NO. 8, pp. 2400-2405, August, 2005.

[47] D. G. Dudley, & H. Y. Pao, "A Parametric Model for Wirless Propagation Channels in Tunnels," *IEEE Antennas and Propagation Society International Symposium*, vol. 1A, NO. 8, pp. 371-374, 2005..